Model validation for a noninvasive arterial stenosis detection problem

H.T. Banks, Shuhua Hu and Zackary R. Kenz
Center for Research in Scientific Computation
North Carolina State University, Raleigh, NC 27695-8212
Carola Kruse, Simon Shaw, and John Whiteman
{carola.kruse, simon.shaw, john.whiteman}@brunel.ac.uk
BICOM, Brunel University, Uxbridge, UB8 3PH, England.
www.brunel.ac.uk/bicom
M.P. Brewin, S.E. Greenwald
{s.e.greenwald, m.p.brewin}@qmul.ac.uk
Blizard Institute, Barts and the London School of Medicine and Dentistry,
Queen Mary, University of London, England.
M. J. Birch
m.j.birch@qmul.ac.uk
Clinical Physics, Barts Health Trust, England.

December 19, 2012

Abstract

A current thrust in medical research is the development of a non-invasive method for detection, localization, and characterization of an arterial stenosis (a blockage or partial blockage in an artery). A method has been proposed to detect shear waves in the chest cavity which have been generated by disturbances in the blood flow resulting from a stenosis. In order to develop this methodology further, we use both one-dimensional pressure and shear wave experimental data from novel acoustic phantoms to validate corresponding viscoelastic mathematical models, which were developed in a concept paper [8] and refined herein. We estimate model parameters which give a good fit (in a sense to be precisely defined) to the experimental data, and use asymptotic error theory to provide confidence intervals for parameter estimates. Finally, since a robust error model is necessary for accurate parameter estimates and confidence analysis, we include a comparison of absolute and relative models for measurement error.

Mathematics Subject Classification: 62F12; 62F40; 65M32; 74D05.

Key words: viscoelastic model; sensitivity analysis; inverse problem; asymptotic theory.

1 Introduction

Coronary artery disease (CAD) is an increasingly prevalent medical condition, and is often a precursor to and cause of a patient experiencing cardiac arrest. Current methods for detection of arterial stenoses (blocked arteries) include the angiogram and CT scans. Angiograms are viable but quite invasive, while CT scans are expensive, introduce radiation into the patient, and can only detect hard plaques (blockages). A desirable new detection method would be noninvasive and less expensive but still effective. To this end, using acoustic waves generated by stenoses has been proposed as a possible detection method [1, 3, 20, 23, 24]. This would place sensors on the surface of the chest to listen for sounds from coronary arteries, with the hope of detecting and then localizing any blockages.

In keeping with [3], we note that the entire system couples two processes: (1) the generation of pressure and shear waves transmitted into the body by the arterial wall as a result of the turbulent blood flow generated by a stenosis, and (2) the propagation of pressure and shear waves through the chest to sensors attached to the chest wall. The first process is not completely understood, though some basic ideas are present in the literature. The current understanding [3, 20] is that turbulent flow produces normal forces on the vessel walls at and downstream of a stenosis, which then exert pressure on the vessels wall causing a small displacement in the surrounding soft tissue. Previous work (e.g. [1, 20, 21, 24]) has demonstrated the existence of such sounds, and [23] discusses past work done on building devices to detect sounds from coronary arteries. As has been noted in previous work (see, e.g., [3, 20]), the focus in practice is on detecting shear waves, due in part to the fact that faster pressure waves have a wavelength that is too long for the distance scales in the body and the corresponding observations that the speed and frequency of shear waves generated by a stenosis are all sufficiently low enough to make shear sound detection plausible.

In terms of the second process, propagation through the chest cavity, it is also known that sounds from coronary stenoses have been sufficiently strong to be detected; although rare, [23] notes that sounds from coronary stenoses have been heard with a stethoscope. The difficulty in detecting these sounds is that they are weaker than other sounds such as heart valves and sounds from coronary arteries which compete with other complex sounds generated by the body (including larger vessels such as carotid arteries). The sounds also attenuate during their passage through the body to the chest wall, which makes them difficult to detect without a deeper understanding of the physics underlying the wave propagation through the chest (hence the need for mathematical models). The approach taken by the work summarized in [23] is treating the problem as a signal-to-noise problem where the signal is weak relative to the noise. In a line of work by Banks, et. al., [3, 12, 13, 14, 15, 19, 22], the sound propagation problem was approached from a mathematical modeling standpoint. Though signal processing would likely be an important component of a diagnostic device, the approach taken in the Banks, et. al., line of work was to build models to describe the underlying physics of sound propagation. These models allow for a characterization of coronary stenoses, which will assist in uncovering these particular coronary artery sounds from the noisy background in the body. Initial experiments were conducted where a gel mold was built with a hose running through the middle; cases where the hose was unblocked were compared to those with blockages, and the results suggested that there were significant differences in sound generation between the blocked and unblocked cases. Unfortunately, this line of work ended before experimental data could be incorporated and fitted to models. The current work picks up the Banks, et. al., ideas, starting again with a one dimensional model and experimental setup.

In this document, we continue the work of our concept paper [8] by focusing on wave propagation through a viscoelastic medium. Here we develop a slightly more general constitutive relationship than in our concept paper, use this constitutive relationship in one-dimensional pressure and shear wave dynamical models, and demonstrate successful inverse problem results for the one-dimensional case using experimental data from a tissue-mimicking gel mold. This data comes from novel acoustic phantoms built at Queen Mary, University of London (QMUL) and Barts Health Trust (BHT) in England. We will examine both the pressure and shear cases to provide evidence of the fidelity of our model fit to data.

2 Experimental Setup

We begin with a discussion of the experimental setup. Two separate novel experiments have been devised at QMUL to gather pressure and shear data; though we will discuss them together, the experiments are run at completely different times and with slightly different phantoms. Devices have been designed (see left panes of Figures 1-2), in which an agar gel mold phantom (homogeneous, 97% water, density $\rho = 1010$ kg/m^3) is loaded

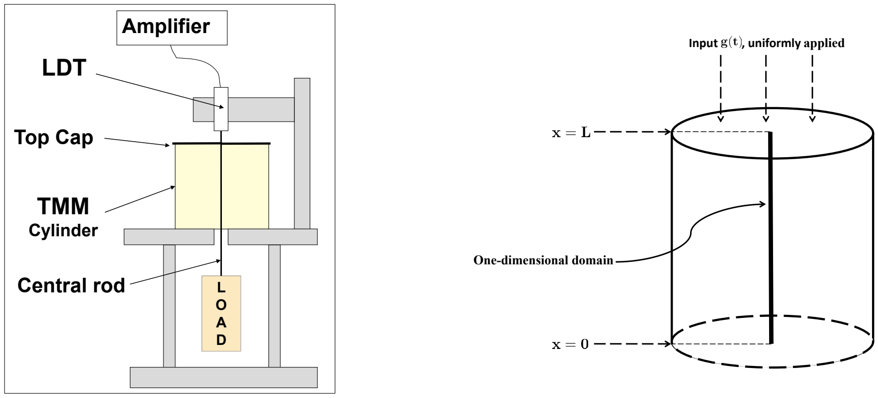

Figure 1: Pressure configuration, where TMM denotes the tissue mimicking material and LDT denotes the laser displacement transducer. (left) Experimental setup of agar phantom. (right) Schematic with one-dimensional domain denoted.

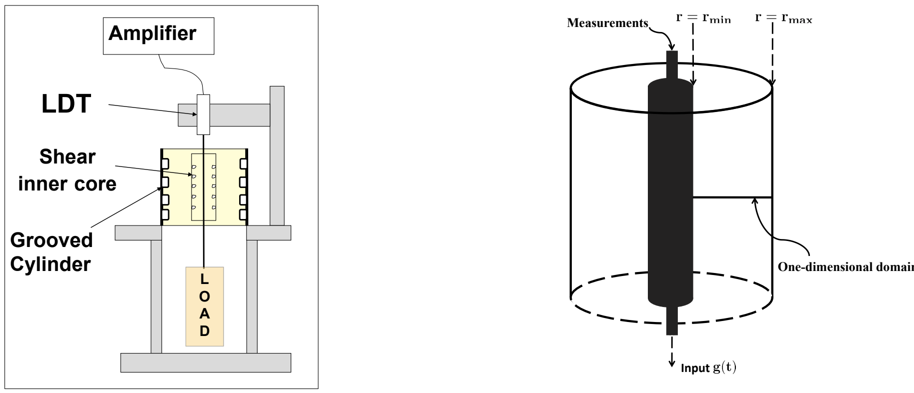

Figure 2: Shear configuration, where again TMM denotes the tissue mimicking material and LDT denotes the laser displacement transducer. (left) Experimental setup of agar phantom. (right) Schematic with one-dimensional domain denoted.

into the rig, a weight is attached applying stress to the phantom, and then the weight is released, causing the material to oscillate. The displacement motion of the material throughout the experiment is measured with a laser device. The choice of loading and a quick release is designed to produce dynamic data; the idea was inspired in part by the impacts the stenosed vessel wall experiences with each heartbeat and also by past success in gathering shear data for filled rubber elastomers using an initially loaded rubber sample which then underwent an impulsive hammer hit (see e.g. [12, 13]). This yields one dimensional pressure data along the vertical axis in the pressure case (right pane of Figure 1) and, in the second experiment, shear data in the radial direction perpendicular to the vertical axis (right pane of Figure 2).

In order to test the phantom response to different stress levels, weights of 66 g, 132 g, 198 g, and 264 g were used in the experiment. The gel phantoms were stored in water when not in use, which keeps the gel at the desired 97% water composition. We will only use data from the 264 g tests later when demonstrating results.

When the experiment is conducted, data like those depicted in Figure 3 are produced. The material is at rest, a weight is added and allowed to settle, then the string holding the weight weight is rapidly cut with a flame to allow the material to freely oscillate. Once oscillations have died out the material relaxes back toward a stable state. The key pieces that will be modeled are the loading profile (loading begins at $t = \Gamma_1$ and lasts until the weight begins to be released at $t = \Gamma_3$), which we will model as instantaneous loading to position A, and the oscillations after weight release (free oscillations begin at $t = \Gamma_4 = 0$) which are the main object of investigations here.

With the setup of the experiment in mind, we can turn to our mathematical model of wave propagation. The model will be developed to take into account all features of the data, including the loading profile and the relaxation present in data. For more information on the experimental setup, interested readers may refer to [17].

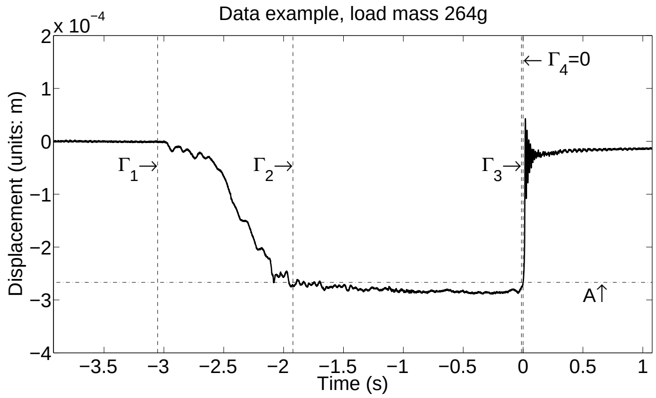

Figure 3: Sample one-dimensional data. Loading of the material (initially at rest) begins at $t = \Gamma_1$, and the material is loaded and continuing to relax for $t \in (\Gamma_2, \Gamma_3)$. At time Γ_3 the load is cut which takes roughly 10 ms–15 ms. The gel is then freely oscillating at $\Gamma_4 = 0$, and oscillations continue for a period of time dependent on the loading weight and wave type (pressure/shear). The value A is the displacement of the material at the beginning of free oscillations. The overall displacement scale of the data is on the order of 10^{-4} m, while the oscillations immediately after the weight release are on the order of 10^{-5} m.

3 Model Development and Constitutive Equation

Since our phantom is cylindrical, the model development begins with three-dimensional equations of motion in cylindrical coordinates. These are given in [22, p.20], and also in [19], and are derived from momentum and mass balance principles. Using the fact that the gel is homogeneous in both the pressure and shear cases and that there are symmetries in the experimental design, these three-dimensional equations can be reduced to simplified one-dimensional models for both cases. In the pressure displacement case, the governing partial differential equation (PDE) becomes

$$\begin{aligned} &\rho \frac{\partial^2}{\partial t^2} u(x,t) - \frac{\partial}{\partial x}\sigma(x,t) = 0 \\ &u(0,t) = 0, \quad \sigma(L,t) = -g(t) \\ &u(x,\Gamma_1) = 0, \quad u_t(x,\Gamma_1) = 0 \end{aligned} \tag{1}$$

where ρ is the density of the material, the stress tensor σ is given by the constitutive relationship for the material (the form of which will be discussed later), $g(t)$ is a function that describes the loading process (again, to be discussed later), and the material is initially at rest. The value $u(x,t)$ represents the displacement of the material at position x and time t, with $x \in (0, L)$ and $t > \Gamma_1$. The time Γ_1 is chosen as the beginning of any stress-strain history in the material; we are assuming the material has been at rest long enough that it is only affected by displacements for $t > \Gamma_1$, where Γ_1 is the time when we start modeling the material history. For our device, $L = 0.0518$ m is the height of the phantom.

In the shear displacement case, the governing equation becomes

$$\begin{aligned} &\rho \frac{\partial^2}{\partial t^2} u(r,t) - \frac{\partial}{\partial r}\sigma(r,t) - \frac{\sigma(r,t)}{r} = 0 \\ &\sigma(r_{min},t) = g(t), \quad u(r_{max},t) = 0 \\ &u(r,\Gamma_1) = 0, \quad u_t(r,\Gamma_1) = 0 \end{aligned} \tag{2}$$

where ρ, σ, and $g(t)$ are analogous to the pressure case and where $r \in (r_{min}, r_{max})$ for $t > \Gamma_1$. For our device, $r_{min} = 0.0105$ m and $r_{max} = 0.054$ m. Throughout this work, we will use r as the spatial variable when the model is for shear displacement and x as the spatial variable for pressure displacement.

In order to complete these models, we must provide a form for σ. This is the constitutive relationship, also called the stress-strain law since it relates strain ($\frac{\partial u}{\partial x}$ or $\frac{\partial u}{\partial r}$) and/or the strain rate to stress σ. The next sections discuss this aspect of the model.

3.1 Constitutive Equation

We incorporate the previous modeling ideas together into a new constitutive equation for the pressure (1) and shear (2) wave PDEs. Throughout this section, the constitutive relationship form is the same for the pressure and shear cases, so x and r are interchangeable unless otherwise noted; for notational convenience, we use x as the spatial variable in the discussion which follows.

3.1.1 Fung Model

Some of the initial investigation into the viscoelastic nature of tissue was completed by Fung (see [7] and the references therein). His work is of particular interest because it was validated in actual tissue. Fung developed a "quasi-linear" model

$$\sigma(t) = \int_{\Gamma_1}^{t} G(t-s) \frac{d\sigma^e(\lambda(s))}{ds} ds \tag{3}$$

with a kernel of the form

$$G(t) = \frac{1 + c\int_{\tau_1}^{\tau_2} \frac{1}{\tau} \exp(-t/\tau) d\tau}{1 + c\ln(\tau_2/\tau_1)}. \tag{4}$$

Within (3), λ represents the stretch of a material ($\lambda = 1 + u_x$) and σ^e describes the elastic response to the elongation λ, given by (see [3])

$$\sigma^e(\lambda) = -\beta + \beta e^{\alpha u_x}$$

where α and β are constants to be estimated (and where we use u_r in the shear case). The parameters τ_i are lower and upper bounds on *relaxation times*, which describe the ways in which the material responds to imposed stresses and strains. This model incorporates a continuum $\tau \in [\tau_1, \tau_2]$ of relaxation times, which Fung found to be necessary in order for his model to match the response of tissue, as well as a constant term in the kernel. This Fung kernel will serve as a baseline which we will refer back to when developing the model for this paper.

3.1.2 Linearized constitutive equation

In this section, we begin by developing the constitutive equation assuming that we will be solving the model starting at $t = \Gamma_1$ and thus incorporating both the loading process and oscillations into our dynamic equations. In Section 3.1.5, we will make an approximation to the loading process which will allow us to focus on the dynamic oscillations of the material after the weight is released, which is our true interest.

To begin, we use the first two terms of the Taylor expansion of $e^{\alpha u_x}$ to approximate

$$\sigma^e \approx -\beta + \beta(1 + \alpha u_x) = \beta\alpha u_x = \gamma u_x \tag{5}$$

where we have combined $\gamma = \beta\alpha$ into a single parameter to be estimated; γ will be incorporated into other parameters later in model development. We can then linearize (3) by using (5), add a Kelvin-Voigt damping term (a common linear viscoelastic damping model [7]), and obtain

$$\sigma(t) = E_1 u_{xt} + \gamma \int_{\Gamma_1}^{t} G(t-s) \frac{du_x(s)}{ds} ds \tag{6}$$

where $G(t)$ is a kernel to be specified. To an extent, the Kelvin-Voigt term describes the overall nature of the damping present in the material, while the kernel $G(t)$ will incorporate different material responses at both the macroscopic and microscopic levels.

3.1.3 Existence and uniqueness for pressure and shear models

Before moving on to the specific form of the constitutive equation kernel, we first establish existence and uniqueness for the pressure (1) and shear (2) equations with the constitutive equation (6). To that end, we set up a similar framework as in the concept paper [8] and connect those results to the current work. We will require that the following assumptions hold:

(A1) The boundary condition function satisfies $g \in L^2(\Gamma_1, T)$;

(A2) The kernel G is differentiable with respect to $t \in \mathbb{R}^+$ and with constants c_1 and c_2 such that $|G(t)| \leq c_1$ and $|\dot{G}(t)| \leq c_2$ for all $t \in \mathbb{R}^+$.

Pressure case

The pressure PDE (1) with constitutive equation (6) are of the same form as those in Section 2 of [8], except that here we have the initial time denoted as $t = \Gamma_1$ instead of $t = 0$ and slightly different variable names (inconsequential changes).

Let $\mathbb{H} = \mathcal{L}^2(0, L)$, $\mathbb{V} = \{\phi | \phi \in \mathcal{H}^1(0, L), \phi(0) = 0\}$, and $\mathbb{V}^*$ denote the topological dual space of $\mathbb{V}$. We identify $\mathbb{H}$ with its topological dual $\mathbb{H}^*$ and thus obtain $\mathbb{V} \hookrightarrow \mathbb{H} = \mathbb{H}^* \hookrightarrow \mathbb{V}^*$ as a Gelfand triple [2, 25]. The notation $\langle \cdot, \cdot \rangle$ denotes the inner product in $\mathbb{H}$, and $\langle \cdot, \cdot \rangle_{\mathbb{V}^*,\mathbb{V}}$ represents the duality pairing between $\mathbb{V}^*$ and $\mathbb{V}$. Let $\mathcal{C}_w(\Gamma_1, T; \mathbb{V})$ denote the set of weakly continuous functions in $\mathbb{V}$ on $[\Gamma_1, T]$, and $\mathcal{L}_T = \{v : [\Gamma_1, T] \to \mathbb{H} \mid v \in \mathcal{C}_w(\Gamma_1, T; \mathbb{V}) \cap \mathcal{L}^2(\Gamma_1, T; \mathbb{V})$ and $v_t \in \mathcal{C}_w(\Gamma_1, T; \mathbb{H}) \cap \mathcal{L}^2(\Gamma_1, T; \mathbb{V})\}$. The notion of weakly continuous (i.e., $u^m \to u$ in $\mathcal{C}_w(\Gamma_1, T; \mathbb{V})$) means that $u^m \to u$ weakly in $\mathbb{V}$ and uniformly in $t \in [\Gamma_1, T]$. Then a weak solution $u \in \mathcal{L}_T$ for the pressure equation must satisfy

$$\begin{aligned}0 &= \rho\langle u_t(t), \eta_t(t)\rangle - \rho \int_{\Gamma_1}^t \langle u_s(s), \eta_s(s)\rangle ds + \int_{\Gamma_1}^t g(s)\eta(L, s) ds + E_1 \int_{\Gamma_1}^t \langle u_{sx}(s), \eta_x(s)\rangle ds \\ &+\gamma \int_{\Gamma_1}^t \left\langle \int_{\Gamma_1}^s G(s-\xi) \frac{d}{d\xi} u_x(\xi) d\xi, \eta_x(s) \right\rangle ds\end{aligned} \tag{7}$$

for any $t \in [\Gamma_1, T]$ and $\eta \in \mathcal{L}_T$. Here and elsewhere $u(t)$ and $\eta(t)$ denote the functions $u(\cdot, t)$ and $\eta(\cdot, t)$, respectively. With these definitions, we still have that the following theorem (a restatement of Theorem 2.2 in [8]) holds:

Theorem 3.1. *Assuming (A1) and (A2), the pressure equation* (1) *with the constitutive relation* (6) *has a unique weak solution on any finite interval* $[\Gamma_1, T]$.

Shear case

This requires a bit more consideration. The shear domain is $\Omega = [r_{min}, r_{max}]$, and is solved on the time frame $t \in [\Gamma_1, T]$. We must slightly redefine the spaces from above to fit the shear model. Let $\mathbb{H} = \mathcal{L}^2(r_{min}, r_{max})$, $\mathbb{V} = \{\phi | \phi \in \mathcal{H}^1(r_{min}, r_{max}), \phi(r_{max}) = 0\}$, and $\mathbb{V}^*$ denote the topological dual space of $\mathbb{V}$. We identify $\mathbb{H}$ with its topological dual $\mathbb{H}^*$ and thus again obtain $\mathbb{V} \hookrightarrow \mathbb{H} = \mathbb{H}^* \hookrightarrow \mathbb{V}^*$ as a Gelfand triple. Let $\mathcal{C}_w(\Gamma_1, T; \mathbb{V})$ denote the set of weakly continuous functions in $\mathbb{V}$ on $[\Gamma_1, T]$, and $\mathcal{L}_T = \{v : [\Gamma_1, T] \to \mathbb{H} \mid v \in \mathcal{C}_w(\Gamma_1, T; \mathbb{V}) \cap \mathcal{L}^2(\Gamma_1, T; \mathbb{V})$ and $v_t \in \mathcal{C}_w(\Gamma_1, T; \mathbb{H}) \cap \mathcal{L}^2(\Gamma_1, T; \mathbb{V})\}$. Then a weak solution $u \in \mathcal{L}_T$ for the shear equation must satisfy

$$\begin{aligned}0 &= \rho\langle u_t(t), \eta_t(t)\rangle - \rho \int_{\Gamma_1}^t \langle u_s(s), \eta_s(s)\rangle ds + \int_{\Gamma_1}^t g(s)\eta(r_{min}, s) ds + E_1 \int_{\Gamma_1}^t \langle u_{sr}(s), \eta_r(s)\rangle ds \\ &+\gamma \int_{\Gamma_1}^t \left\langle \int_{\Gamma_1}^s G(s-\xi) \frac{d}{d\xi} u_r(\xi) d\xi, \eta_r(s) \right\rangle ds - E_1 \int_{\Gamma_1}^t \int_{r_{min}}^{r_{max}} \frac{u_{rt}(r,s)}{r} \eta(r,s) dr ds \\ &-\gamma \int_{\Gamma_1}^t \int_{r_{min}}^{r_{max}} \left(\int_{\Gamma_1}^s \frac{1}{r} G(s-\xi) \frac{du_r(r,s)}{d\xi} d\xi \right) \eta(r,s) dr ds\end{aligned} \tag{8}$$

for any $t \in [\Gamma_1, T]$ and $\eta \in \mathcal{L}_T$ and where $\langle \cdot, \cdot \rangle$ is the usual inner product. Since $r_{min} > 0$, there are no singularities in the final term in (8), and the kernel integral in the numerator of that term will converge in the same manner as the preceding kernel integral. Thus, the arguments from [8] for the pressure case apply in the shear case, and we have the following theorem:

Theorem 3.2. *Assuming (A1) and (A2), the shear equation* (2) *with constitutive relationship* (6) *has a unique weak solution on any finite interval* $[\Gamma_1, T]$.

3.1.4 Form for constitutive equation kernel $G(t)$

We will now state the particular kernel used for this current work, and then manipulate it into a form that gives more physical insight and which will later allow for a conceptual framework using *internal variables.* We develop this kernel from a different perspective than that given in [8], but the resulting form will be quite similar. Using the notation and parameter conventions of [7], we define the kernel in this work to be

$$G(t; P) = \kappa_r + K(t; P) \tag{9}$$

where κ_r is a constant representing an instantaneous relaxation modulus (justified by the fact that our gel phantom acts partly as a solid) and $K(t; P) = \int_{\mathcal{T}} \exp(-t/\tau) dP(\tau)$ represents a continuum of distributed relaxation times with $\mathcal{T} = [\tau_1, \tau_2] \subset (0, \infty)$ and where $P(\tau)$ is a probability measure on $\mathcal{T}$. Note that this form for G satisfies $|G(t)| \leq c_1$ with G clearly differentiable and $|\dot{G}(t)| \leq c_2$ for some constants c_1, c_2 so that assumption (A2) is satisfied. It is also worth noting here that our proposed kernel form (9) is similar to that in Fung's model (4), as we see that κ_r serves as an analog to the constant portion of Fung's kernel (i.e., $\frac{1}{1 + c\ln(\tau_1/\tau_1)}$) and the $K(t; P)$ portion is similar to the the continuous relaxation spectrum in Fung's model (i.e., $\frac{c\int_{\tau_1}^{\tau_2} \frac{1}{\tau}\exp(-t/\tau)d\tau}{1 + c\ln(\tau_2/\tau_1)}$).

We substitute (9) into (6) and manipulate the form of the stress, noting that $u_x(\Gamma_1) = 0$ since the material is initially at rest and using the fact that that $K(0; P) = 1$:

$$
\begin{aligned}
\sigma(t; P) &= E_1 u_{xt} + \gamma \int_{\Gamma_1}^{t} G(t-s) \frac{du_x(s)}{ds} \\
&= E_1 u_{xt} + \gamma \int_{\Gamma_1}^{t} \left(\kappa_r + K(t-s; P)\right) \frac{du_x(s)}{ds} \\
&= E_1 u_{xt} + \kappa_r \gamma \int_{\Gamma_1}^{t} \frac{d}{ds} u_x(s) ds + \gamma \int_{\Gamma_1}^{t} K(t-s; P) \frac{d}{ds} u_x(s) ds \\
&= E_1 u_{xt} + \kappa_r \gamma \left(u_x(t) - \underbrace{u_x(\Gamma_1)}_{0} \right) + \gamma \int_{\Gamma_1}^{t} K(t-s; P) \frac{d}{ds} u_x(s) ds \\
&= E_1 u_{xt} + \kappa_r \gamma u_x(t) + \gamma \int_{\Gamma_1}^{t} K(t-s; P) \frac{d}{ds} u_x(s) ds \\
&= E_1 u_{xt} + E u_x(t) + \gamma \left(K(0; P) u_x(t) - \underbrace{K(t; P) u_x(\Gamma_1)}_{0} - \int_{\Gamma_1}^{t} \frac{\partial K(t-s; P)}{\partial s} u_x(s) ds \right) \\
&= (E + \gamma)\, u_x(t) + E_1 u_{xt}(t) - \gamma \int_{\Gamma_1}^{t} \frac{\partial K(t-s; P)}{\partial s} u_x(s) ds \qquad (10)
\end{aligned}
$$

where $E = \kappa_r \gamma$. This equation (10) is the general form of the constitutive equation used here. The value $E_0 = E + \gamma$ can be considered to be a dynamic analog to the static Young's modulus in the pressure case or the static shear modulus in the shear case; this also makes clear the fact that Hooke's Law is incorporated into our model. We have already discussed that E_1 is the bulk damping parameter for the Kelvin-Voigt damping term. The final integral represents a history term which describes the relaxation of the material in response to an applied stress/strain.

We will ultimately turn to a discretized distribution model (using a discrete measure $P(\tau)$), and connect it to the continuum model through a probability measure approximation as in [4]. This will allow us to develop a computationally feasible inverse problem, and also give insight into the underlying material mechanics. But first we briefly discuss a method for approximating the loading process.

3.1.5 Approximating the loading process

Recalling Figure 3, the loading profile is relatively long compared with the oscillatory period; since our concern is with modeling the oscillations, solving the model from Γ_1 is much longer than necessary. Also, early experimentation with the model indicated that the parameters governing the loading and resting process may differ from those governing the very dynamic post-release oscillatory process.

We address these concerns by modeling the loading as instantaneous from at rest to a displacement of A at position $x = L$ or $r = r_{min}$. Since the material is linear, this would then mean the phantom has the profile $u(x,t) = \frac{A}{L}x$ in the pressure case and $u(r,t) = \frac{A(r_{max} - r)}{r_{max} - r_{min}}$ in the shear case, up until the time of the weight release. Since this is an approximation, we will neglect the times $t \in (\Gamma_3, \Gamma_4)$, the weight release time period, since that time frame is small relative to the loading and settling time from Γ_1 to Γ_3. We also incorporate a time parameter Υ which will represent our approximation of the time when loading begins. In the formulation here we will use the same relaxation times during the loading process as during the oscillation period, which means that Υ has no meaning other than as a tuning parameter that we must estimate. Thus, we assume the given loading profiles for $t \in (\Upsilon, 0)$ since $\Gamma_4 = 0$ in our convention. This also means that $\Upsilon < 0$.

We incorporate this loading approximation into our model by manually integrating the constitutive relationship (10). For the purposes here, we will call $\hat{\sigma}$ the full constitutive relationship for $t > \Upsilon$ that is described by (10) (where we now use Υ in the place of Γ_1), and σ the constitutive relationship for $t > 0$. We do this for notational simplicity in the final model, at the expense of some minor notational confusion at the current stage.

For the pressure case, we compute (noting that $u(x,t) = \dfrac{A}{L}x$ implies $u_x(x,t) = A/L$, for $\Upsilon < t < 0$)

$$\begin{aligned}
\hat{\sigma}(t;P) &= (E+\gamma)\,u_x(t) + E_1 u_{xt}(t) - \gamma\int_{\Upsilon}^{t}\frac{\partial K(t-s;P)}{\partial s}u_x(s)ds \\
&= (E+\gamma)\,u_x(t) + E_1 u_{xt}(t) - \gamma\int_{\Upsilon}^{0}\frac{\partial K(t-s;P)}{\partial s}u_x(s)ds - \gamma\int_{0}^{t}\frac{\partial K(t-s;P)}{\partial s}u_x(s)ds \\
&= (E+\gamma)\,u_x(t) + E_1 u_{xt}(t) - \gamma\int_{\Upsilon}^{0}\frac{\partial K(t-s;P)}{\partial s}\frac{A}{L}ds - \gamma\int_{0}^{t}\frac{\partial K(t-s;P)}{\partial s}u_x(s)ds \\
&= (E+\gamma)\,u_x(t) + E_1 u_{xt}(t) - \gamma\frac{A}{L}(K(t;P) - K(t-\Upsilon;P)) - \gamma\int_{0}^{t}\frac{\partial K(t-s;P)}{\partial s}u_x(s)ds \\
&= \sigma(t;P) - \mathcal{F}(t;\Upsilon,A,P)
\end{aligned}$$

where $\mathcal{F}(t;\Upsilon,A,P) = \gamma\dfrac{A}{L}(K(t;P) - K(t-\Upsilon;P))$ and

$$\sigma = (E+\gamma)\,u_x(t) + E_1 u_{xt}(t) - \gamma\int_{0}^{t}\frac{\partial K(t-s;P)}{\partial s}u_x(s)ds \qquad (11)$$

incorporates the remaining terms and represents the constitutive relationship for $t > 0$. For the pressure setup, we then have the following:

- $\hat{\sigma}_x = \sigma_x$
- The original stress boundary condition is $\hat{\sigma}(L,t;P) = 0$. Using the preceding development, this corresponds with

  $$0 = \sigma(L,t;P) - \mathcal{F}(t;\Upsilon,A,P)$$

  which allows us to write the boundary condition for a model solved for $t > 0$ as

  $$\sigma(L,t;P) = \mathcal{F}(t;\Upsilon,A,P).$$

  Since $A, \Upsilon < 0$ and $\gamma > 0$, we know that $K(t;P) - K(t-\Upsilon;P) > 0$. Hence, since $L > 0$, we have a compressive boundary stress, which is what we would expect in the pressure case.

The shear case is similar. For the loading profile $u(r,t) = \frac{A(r_{max}-r)}{r_{max}-r_{min}}$ for $t \in (\Upsilon, 0)$, we have $u_r(r,t) = -\frac{A}{r_{max}-r_{min}}$ which is incorporated when integrating the history in the same way as the pressure case. We then find the corresponding loading stress to be $\mathcal{F}(t;\Upsilon,A,P) = -\zeta\frac{A}{r_{max}-r_{min}}(K(t;P) - K(t-\Upsilon;P)$, where ζ is the shear analog to γ. Also, we have $\hat{\sigma}_r = \sigma_r$ as in the pressure case. However, we have the term $\dfrac{\hat{\sigma}}{r} = \dfrac{\sigma}{r} - \dfrac{\mathcal{F}(t;\Upsilon,A,P)}{r}$, which will result in a time-dependent forcing term in the shear PDE.

We make two comments before discussing the internal variable forms. First, if we assume, for example, a single relaxation time and that its value is small, say on the order of 10^{-1}, then the term $K(t-\Upsilon;P) = \exp(-(t-\Upsilon)/\tau_1) \approx \exp(-10(t-\Upsilon))$ attains its maximum value $\exp(10\Upsilon)$ when $t = 0$. Note that for, say, $\Upsilon < -1$, this term is negligible. Relaxation times on this order are what we can later obtain in the inverse problem, which would imply that in our case the material is at rest after being loaded sufficiently long that it "forgets" its loading history by the time the weight is released. This is good from an experimental standpoint, since the loading process will never be quite uniform. It is also good to know from a computational perspective; we can limit Υ to being greater than some value, such as $-20 < \Upsilon < 0$, which will keep the optimization algorithm from marching off unnecessarily (which occurred in some of our early inverse problem tests). Second, since we have integrated out the loading history, we now start the model at the time of weight release, $t = 0$. This means that the material is considered at rest just prior to the release; thus, in the history integrals we will discuss in the next section, all the history now starts at $t = 0$ since the history before that point will be incorporated into the initial loading profile and an initial stress condition.

3.1.6 Internal Variables

In the previously noted work on this stenosis problem, the double integrals that resulted from using the continuum of relaxation times in the stress equation were computationally intractable so another approach was required. The idea was to use a discrete number of internal variables. As will be noted, these gave rise to a differential form which was an improvement computationally since it led to purely differential equations in the model rather than inclusion of an integro-differential equation. With the advances in desktop computation abilities since that time, the integral form is now reasonable to use in a dynamic model. However, internal variables are still attractive in that they provide a formulation that indicates some of the internal material dynamics. Physically, if we assume that the molecules within the biological tissue are on a microscopic scale then the portion of the material which is represented by each internal variable or internal strain ϵ_j is being driven by the overall strain and has a response that varies depending on the value of the corresponding relaxation time τ_j.

One of the earlier constitutive relationship formulations, in [3, 19, 22], approximates the Fung kernel as a finite sum of exponential functions

$$G(t) = \sum_{j=1}^{N} C_j \exp\left(-t/\tau_j\right)$$

where C_j are weights and τ_j are *relaxation times* that describe how the material relaxes after undergoing deformation. If one uses this form for $G(t)$ in the constitutive relationship (3), one still must compute the integral in

$$\sigma(t) = \int_0^t \sum_{j=1}^{N} C_j \exp(-(t-s)/\tau_j) \frac{d}{ds}\sigma^e(\lambda(s))ds = \sum_{j=1}^{N} C_j \epsilon_j(t)$$

where $\epsilon_j(t) = \int_0^t \exp(-(t-s)/\tau_j)\frac{d}{ds}\sigma^e(\lambda(s))ds$. We can instead compute each $\epsilon_j(t)$ as a dynamic internal variable following the differential equation (for $j = 1, 2, \ldots, N$)

$$\frac{d\epsilon_j(t)}{dt} + \frac{1}{\tau_j}\epsilon_j(t) = \frac{d\sigma^e(\lambda(t))}{dt}, \quad \epsilon_j(0) = 0.$$

Note that these are then linear differential equations for ϵ_j. One could introduce nonlinearities, which is discussed in [3, 19] and was found to be equivalent to assuming multiple relaxation times; we do not consider nonlinear internal dynamics in this work as we shall see later that the linear constitutive relationship (10) with a discrete measure gives a reasonable approximation to the data provided by QMUL and BHT.

Note, however, that the kernel here is composed of a discrete sum of exponentials. At first glance, this appears to run counter to the Fung results which point toward a continuum of times being important. The results in [3, 19, 22] demonstrate that the internal variable approach is valid and does appear to work as well as the continuum of times in the Fung kernel, but we would like to put this on firmer ground. A connection between the Fung continuum model and the discrete kernel is provided by the work in [14]. The authors there form the kernel

$$G(t) = \int_{\mathcal{T}} q(t;\tau)dP(\tau)$$

where $\mathcal{T} = [\tau_1, \tau_2] \subset (0, \infty)$ is the set of admissible relaxation times, $P(\tau)$ is a probability measure on $\mathcal{T}$, and $q(t;\tau)$ is a continuous function of relaxation times. If we take $q(t;\tau) = \exp(-t/\tau)$, this corresponds with the kernels previously discussed. The authors showed existence and uniqueness results for this kernel in the nonlinear constitutive equation (3). Though this framework is back to the continuous relaxation time case, a result from [4] allows one to approximate any measure $P(\tau)$ with a discrete measure. This discrete measure leads us back to the previous case with a sum of exponentials, but from the probabilistic framework we know conclusively that we are approximating the continuous spectrum of Fung and from the results of [3, 19, 22] we know that this approximation has been viable when implemented.

With this understanding of previous work using internal variables, we move forward by modifying our current model. We manipulate the form of Equation (11) as follows:

$$\begin{aligned}
\sigma(t;P) &= (E+\gamma)\,u_x(t) + E_1 u_{xt}(t) - \gamma \int_0^t \frac{\partial K(t-s;P)}{\partial s} u_x(s)ds \\
&= (E+\gamma)\,u_x(t) + E_1 u_{xt}(t) - \gamma \int_0^t \frac{\partial}{\partial s}\left(\int_{\mathcal{T}} \exp(-(t-s)/\tau)dP(\tau)\right) u_x(s)ds \\
&= (E+\gamma)\,u_x(t) + E_1 u_{xt}(t) - \gamma \int_{\mathcal{T}} \int_0^t \frac{\partial}{\partial s}\left(\exp(-(t-s)/\tau)\right) u_x(s)ds\; dP(\tau) \\
&= (E+\gamma)\,u_x(t) + E_1 u_{xt}(t) - \gamma \int_{\mathcal{T}} \epsilon_1(t;\tau)dP(\tau),
\end{aligned} \tag{12}$$

where in the final step $\epsilon_1(t;\tau) = \displaystyle\int_0^t \frac{\partial}{\partial s}\left(\exp\left(-(t-s)/\tau\right)\right) u_x(s)ds$. Rather than the integral form for ϵ_1, we can use the differential form

$$\tau\frac{d}{dt}\epsilon_1(t;\tau) + \epsilon_1(t;\tau) = u_x(t), \quad \epsilon_1(0;\tau) = 0 \tag{13}$$

which is then solved simultaneously with the rest of the model dynamics. This is then an *internal variable* or *internal strain*, driven by the overall strain $u_x(t)$, which is the continuous form of the internal variable formulation.

We now may finally make the discrete assumption

$$P(\tau) = \sum_{j=1}^{N_p} p_j \Delta_{\tau_j}$$

where Δ_{τ_j} is the Heaviside function with step at τ_j and p_j are the proportions of the material subject to relaxation time τ_j. By substituting this discrete P into the form for σ as developed in (12), we obtain the discrete, internal variable form of the constitutive relationship

$$\sigma(t) = \left(E + \sum_{j=1}^{N_p}\gamma_j\right) u_x(t) + E_1 u_{xt}(t) - \sum_{j=1}^{N_p}\gamma_j \epsilon^j(t), \tag{14}$$

with internal variables obeying (for $j = 1, 2, \ldots, N_p$)

$$\tau_j \frac{d}{dt}\epsilon^j(t) + \epsilon^j(t) = u_x(t), \quad \epsilon^j(0) = 0, \tag{15}$$

and where we have defined $\gamma_j = \gamma p_j$ so that $\gamma = \displaystyle\sum_{j=1}^{N_p}\gamma_j$. Note that we assume $E > 0$, since the agar gel acts at least partly as a solid, and that $\epsilon^j = \epsilon_1(\cdot;t_j)$.

3.2 Final PDE pressure and shear models

We now put together the pressure (1) and shear (2) wave equations, using the constitutive equation (14)-(15) but with the loading history approximation integrated out as discussed in Section 3.1.5. Recall also that the discrete assumption for P and the form of K gives us $\gamma K(t;P) = \gamma \sum_{j=1}^{N_p} p_j \exp(-t/\tau_j) = \sum_{j=1}^{N_p} \gamma_j \exp(-t/\tau_j)$ where $\gamma_j = \gamma p_j$. These equations are just manipulated versions of the general equations of Theorems 3.1-3.2, so we still know a unique weak solution exists on any finite time interval.

Pressure Model

The pressure equations, solved for $t > 0$ which is the release time, are then

$$\begin{aligned}
&\rho\frac{\partial^2}{\partial t^2}u(x,t) - \frac{\partial}{\partial x}\sigma(x,t) = 0 \\
&u(0,t) = 0, \quad \sigma(L,t) = \frac{A}{L}\left[\sum_{j=1}^{N_p}\gamma_j \exp(-t/\tau_j) - \sum_{j=1}^{N_p}\gamma_j \exp(-(t-\Upsilon)/\tau_j)\right] \\
&u(x,0) = \frac{A}{L}x, \quad u_t(x,0) = 0,
\end{aligned} \tag{16a}$$

where

$$\sigma(t) = \left(E + \sum_{j=1}^{N_p} \gamma_j \right) u_x(t) + E_1 u_{xt}(t) - \sum_{j=1}^{N_p} \gamma_j \epsilon^j(t) \tag{16b}$$

with the internal variables subject to (for $j = 1, 2, \ldots, N_p$)

$$\tau_j \frac{d}{dt} \epsilon^j(t) + \epsilon^j(t) = u_x, \quad \epsilon^j(0) = 0. \tag{16c}$$

The parameter ρ still represents the material density and E_1 the damping parameter. E represents an instantaneous relaxation modulus. The γ_j values are weightings on relaxation times τ_j; also, we can write $E_0 = E + \sum_{j=1}^{N_p} \gamma_j$ as the viscoelastic analog to Young's modulus.

Shear Model

We next present the shear equations. In order to more easily distinguish between pressure and shear model parameters, we will use G and G_1 in place of E and E_1 and ζ_j instead of γ_j. We find

$$\begin{aligned}
&\rho \frac{\partial^2}{\partial t^2} u(r,t) - \frac{\partial}{\partial r} \sigma(r,t) - \frac{\sigma(r,t)}{r} = \frac{1}{r} \frac{A}{r_{max} - r_{min}} \left[\sum_{j=1}^{N_p} \zeta_j \exp(-t/\tau_j) - \sum_{j=1}^{N_p} \zeta_j \exp(-(t - \Upsilon)/\tau_j) \right] \\
&\sigma(r_{min}, t) = \frac{-A}{r_{max} - r_{min}} \left[\sum_{j=1}^{N_p} \zeta_j \exp(-t/\tau_j) - \sum_{j=1}^{N_p} \zeta_j \exp(-(t - \Upsilon)/\tau_j) \right], \quad u(r_{max}, t) = 0 \\
&u(r, 0) = \frac{A(r_{max} - r)}{r_{max} - r_{min}}, \quad u_t(r, 0) = 0,
\end{aligned} \tag{17a}$$

where

$$\sigma(t) = \left(G + \sum_{j=1}^{N_p} \zeta_j \right) u_r(t) + G_1 u_{rt}(t) - \sum_{j=1}^{N_p} \zeta_j \epsilon^j(t) \tag{17b}$$

with the internal variables subject to (for $j = 1, 2, \ldots, N_p$)

$$\tau_j \frac{d}{dt} \epsilon^j(t) + \epsilon^j(t) = u_r, \quad \epsilon^j(0) = 0. \tag{17c}$$

We note that $G_0 = G + \sum_{j=1}^{N_p} \zeta_j$ is the dynamic analog of the shear modulus.

3.3 Numerical method

We use the same numerical implementation for both the pressure (16) and shear (17) models, which is also the same as in the concept paper [8]. In time, we use a discontinuous Galerkin method composed of normalized Legendre polynomials (of order 4). In space, we use a continuous spectral finite element method composed of Lagrange basis functions on Gauss-Lobatto nodes (also of order 4). This allows the higher order (4-5th order) elements in space while controlling dispersion error. Under this scheme, the system matrices are diagonalizable – this could be lost if we did not use normalized Legendre polynomials in time. Also, the solver time for the shear model is slower than that for the pressure model due to the time-dependent right hand side. Further details are in a forthcoming BICOM report [18].

4 Inverse Problem

With models in hand, we now turn to matching the model output to data. We will use two common methods in order to estimate model parameters. One is ordinary least squares (OLS) and the other is generalized least squares (GLS). These will be defined later in Section 4.2.

As discussed in Section 2, separate experiments have been designed to gather one-dimensional pressure and shear data. Measurements in our experiment are taken at $x = L$ for the pressure case and $r = r_{min}$ for the shear case, and will be denoted u_j. Corresponding pressure or shear model solutions at the same spatial location will be denoted $u(t_j; 10^\theta)$, where the measurement location has been suppressed so we can retain a general pressure/shear model solution notation and where θ represents a vector of the base-10 logarithm of each parameter (the same idea used previously [8] to reduce parameter scaling issues). Each data set has been trimmed to the dynamic oscillations after the release, and thus the time frame for pressure data is roughly 150ms while that for shear is 200ms, with a data sampling rate of 2.048kHz. Using the full set of data points proved to make the inverse problem difficult and computationally intractable, as that many data points made the inverse problem too overdetermined. Thus, we use the data with a sampling rate of 1.024kHz instead as the full data set. We take n to be the total number of data points for a particular data set, and thus can describe the measurement time points for the full "every data point" set as $t_j = j/1024$ where $j = 0, 1, \ldots, n-1$. There will also be a reduced data set where we take every other data point starting with $t_0 = 0$.

Since some of the data points were near zero in absolute value, we found that those points resulted in scaling problems when using the GLS model to estimate model parameters (since the corresponding cost functional divides by the model value as we will see later when this method is defined). To account for this, we removed from consideration any data points u_j (and their corresponding model solutions at that time point) where $|u_j| < 5 \times 10^{-6}$. This value was chosen by examining the data, noting that the data is on the order of 10^{-5} and that the "jitter" one can see in Figure 3 has a magnitude of roughly 5×10^{-6} during the times before loading up to Γ_1, then during the settling period from Γ_2 to Γ_3, and again in the settling period after the oscillations have died out. Thus, our threshold level is below the level of noise in the data. This level also eliminated only a few data points, while providing significantly improved GLS robustness. The number of data points n is then reduced according to how many thresholded data points were removed.

Before going into the setup and results for the inverse problem, we note that the forward (i.e., direct) problems where we solve for displacement (using the method discussed in Section 3.3) are as follows:

- **Pressure forward problem**: Given E, E_1, τ_j and γ_j for $j = 1, 2, \ldots, N_p$, Υ, A, L, and ρ, solve model (16) for displacement $u(x,t)$ at each position $x \in [0, L]$ for $t \in [0, T]$.

- **Shear forward problem**: Given G, G_1, τ_j and ζ_j for $j = 1, 2, \ldots, N_p$, Υ, A, r_{min}, r_{max}, and ρ, solve model (17) for displacement $u(r,t)$ at each position $x \in [r_{max}, r_{min}]$ for $t \in [0, T]$.

The inverse problems we will develop here are as follows:

- **Pressure inverse problem**: Given pressure displacement data at $x = L$ and a corresponding forward problem solver for displacement, along with specified values for ρ and L, find values for the constants E, E_1, τ_j and γ_j (for $j = 1, 2, \ldots, N_p$), A, and Υ which provide the best fit to the data (in a manner which will be defined shortly).

- **Shear inverse problem**: Given shear displacement data at $r = r_{min}$ and a corresponding forward problem solver for displacement, along with specified values for ρ, r_{min}, and r_{max}, find values for the constants G, G_1, τ_j and ζ_j (for $j = 1, 2, \ldots, N_p$), A, and Υ which provide the best fit to the data (again, in a manner which will be defined shortly).

We assume for both the pressure and shear cases that the parameters lie in some admissible set $Q \subset \mathbb{R}^\kappa$, where Q is assumed to be compact and κ is the number of parameters requiring estimation. Throughout the remainder of this work, we will denote the log-scaled parameter vector for pressure (for $N_p = 1$) as

$$\theta = (\log_{10}(E), \log_{10}(E_1), \log_{10}(\gamma_1), \log_{10}(\tau_1), \log_{10}(-A), \log_{10}(-\Upsilon)) \tag{18}$$

with a similar vector for shear where we use the shear parameters parameters G, G_1, and ζ_1 in place of E, E_1, and γ_1, respectively. Thus, as long as we define our cost function to be a continuous function of the parameters, we know the inverse problem has a solution (minimizing a continuous function on a compact parameter space). One could broaden this parameter estimation framework to the distributional case if desired, taking an admissible parameter space as a compact subset of Euclidean space (including all parameters excuding relaxation times) along with with the space of probability measures, and use the Prohorov metric framework (see, e.g., [9, Sec. 4]) and the approximation results of [4]. This again leads to minimizing a continuous function of the parameters over a compact space. Either way, the inverse problems we will shortly define will have solutions.

4.1 Sensitivity of model output to parameters

We consider the sensitivity of the model output to the parameters (equations are shown in Appendix A). For our examinations here, we will look at both the pressure and shear parameter sensitivities. The weight level is 264g, and we will show results for one relaxation time ($N_p = 1$). Since we estimate the log-scaled parameter values (due to the varying scales of the parameters), we depict here the sensitivities with respect to those log-scaled parameters in Figures 4-5. The particular parameter values at which we solved the sensitivities are located in the figure captions, and are parameters which produce a model solution with roughly the same features (e.g., overall amplitude, wave frequency, damping envelope) as the experimental data.

In the pressure case, the model is most sensitive to E, γ_1, A, and Υ and less sensitive to E_1 and τ_1. In the shear case, the model is most sensitive to G, ζ_1 and A, and less sensitive to G_1, Υ and τ_1. This lower sensitivity to τ_1 in both cases is fully consistent with the results in [8].

4.2 Statistical Models and Parameter Estimators

In order to carefully define the way in which we will measure the closeness of the data to model values, we must first discuss underlying statistical models for the error present in the data. A proper error model is also key to correctly determining parameter confidence intervals. Much of the discussion here is similar to that in [8], with background on ordinary least squares (OLS) and generalized/weighted least squares (GLS or WLS) given in [16], for example.

We will assume the errors $\mathcal{E}_j$ are independent, identically distributed with mean zero ($E[\mathcal{E}_j] = 0$) and constant variance $\text{var}(\mathcal{E}_j) = \sigma_0^2$; this process has realizations ε_j. Note that we do not assume we know the underlying distributions from which the errors come; we only know the first two central moments as specified. We use this error process in proposing two error models and corresponding parameter estimators.

- **Absolute error**: Here we have the error process $U_j = u(t_j; 10^{\theta_0}) + \mathcal{E}_j$, with realizations

$$u_j = u(t_j; 10^{\theta_0}) + \varepsilon_j, \tag{19}$$

where θ_0 is some hypothesized "true" parameter value (see [16]). We use the ordinary least squares cost function

$$\mathcal{J}_{ols}(\theta) = \sum_{j=0}^{n-1} [u_j - u(t_j; 10^{\theta})]^2.$$

The corresponding inverse problem for the logged parameters is then

$$\hat{\theta}_{ols} = \arg\min_{\theta \in Q} \mathcal{J}_{ols}(\theta) = \arg\min_{\theta \in Q} \sum_{j=0}^{n-1} [u_j - u(t_j; 10^{\theta})]^2. \tag{20}$$

This function minimizes the distance between the data and model where all observations are considered to have equal importance (weight). Since $u(t_j; 10^{\theta})$ is a continuous function of θ, $\mathcal{J}_{ols}$ is also a continuous function of θ, which means we are minimizing a continuous function of θ over a compact set Q, and thus this inverse problem has a solution.

- **Relative error**: Here we have the error process $U_j = u(t_j; 10^{\theta_0}) + u(t_j; 10^{\theta_0})\mathcal{E}_j$ with realizations

$$u_j = u(t_j; 10^{\theta_0}) + u(t_j; 10^{\theta_0})\varepsilon_j. \tag{21}$$

For this case, we construct the generalized (weighted) least squares cost function (as per, e.g., [16])

$$\mathcal{J}_{gls}(\theta) = \sum_{j=0}^{n-1} w_j^2 [u_j - u(t_j; 10^{\theta})]^2$$

where we define the weights $w_j = u(t_j; 10^{\theta})^{-1}$. In this case, since we are examining a relative error model (21), these weights take into account the unequal quality of observations; dividing by the function value has a "normalizing" effect on the errors, accounting for the scale differences which may be present in the errors at larger versus smaller model values.

We now wish to find θ such that $\mathcal{J}_{gls}(\theta)$ is minimized. We can either solve this directly, or by using an iterative procedure in order to estimate $\hat{\theta}_{gls}$ (since the weights must also be estimated). We will use an iterative method, described as follows (see [16] and references therein for convergence details):

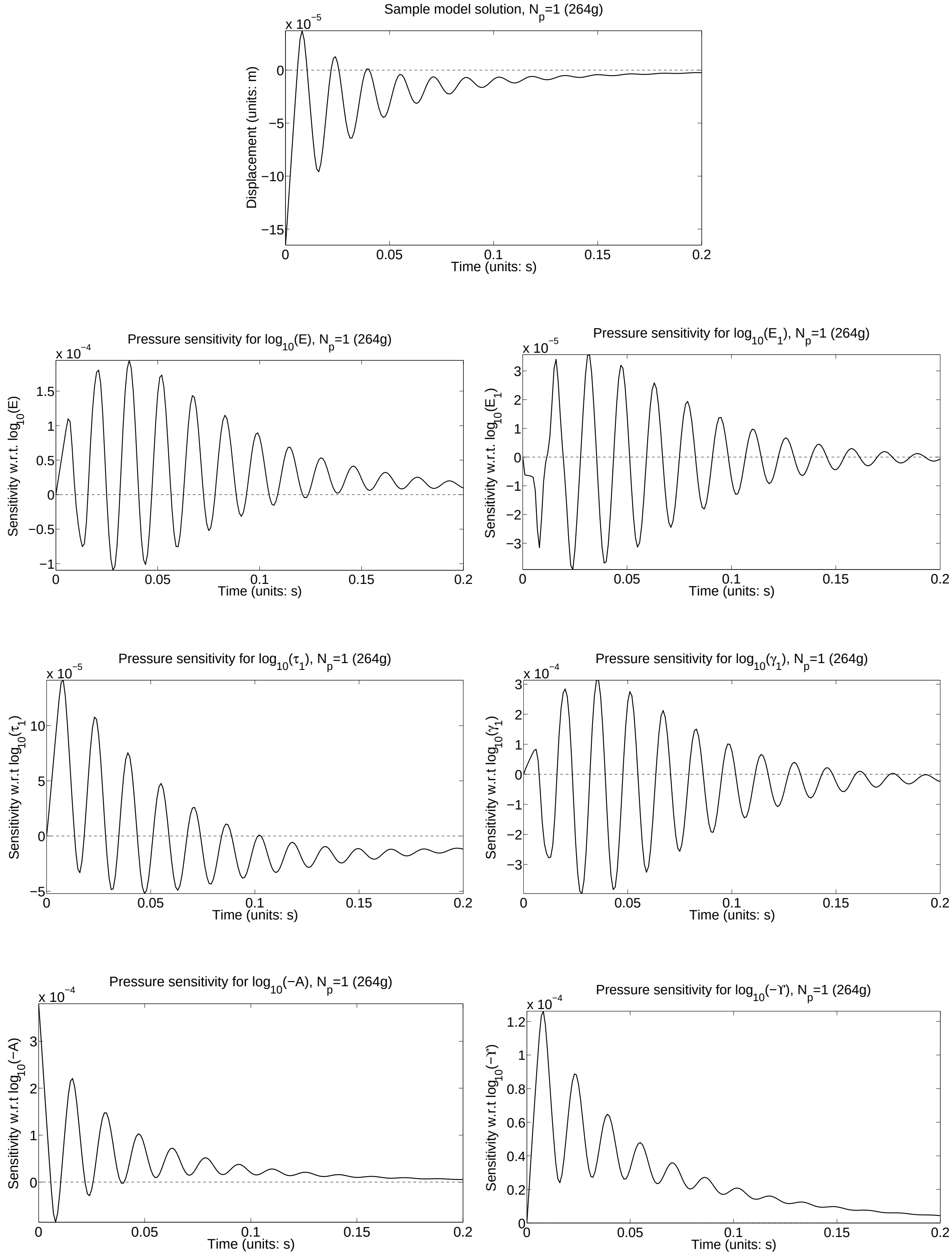

Figure 4: Pressure sensitivity equation solutions in the $N_p = 1$ case. Solved using the following parameter values: $E = 5 \times 10^4$ Pa, $E_1 = 30$ Pa·s, $\gamma_1 = 1.2 \times 10^5$ Pa, $\tau = 0.02$ s, $A = -1.65 \times 10^{-4}$ m, and $\Upsilon = -0.01$ s. (top) Resulting pressure model solution. (bottom six) Sensitivity equation solutions for each parameter.

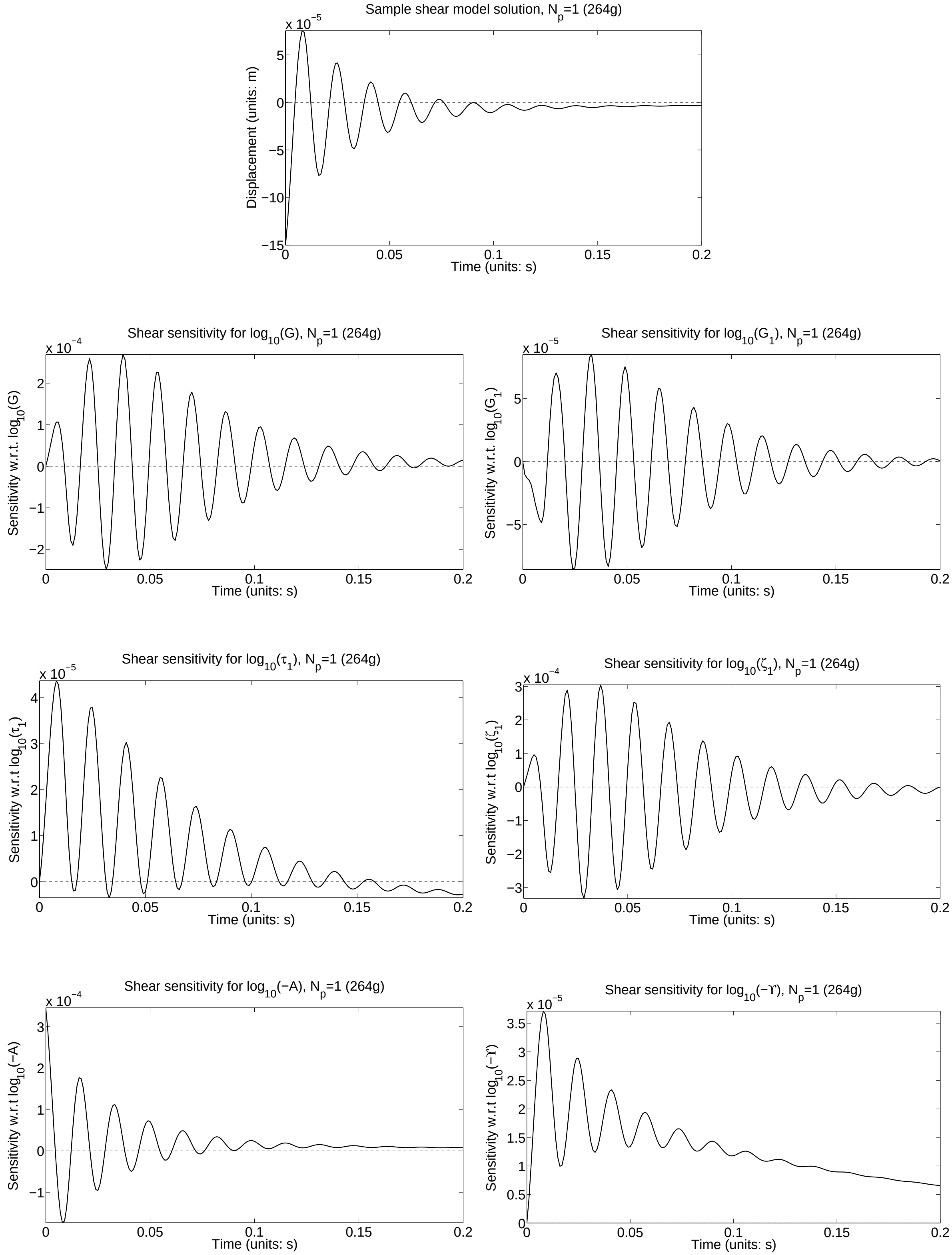

Figure 5: Shear sensitivity equation solutions in the $N_p = 1$ case. Solved using the following parameter values: $G = 6.5 \times 10^3$ Pa, $G_1 = 5.6$ Pa·s, $\zeta_1 = 8 \times 10^3$ Pa, $\tau = 0.07$ s, $A = -1.5 \times 10^{-4}$ m, and $\Upsilon = -0.01$ s. (top) Resulting shear model solution. (bottom six) Sensitivity equation solutions for each parameter.

1. Define $\hat{\theta}^0 = \hat{\theta}_{ols}$, and set $k = 0$.
2. Form the weights $\hat{w}_j = u(t_j; 10^{\hat{\theta}^k})^{-1}$, using weight thresholding (described below).
3. Re-estimate $\hat{\theta}_{gls}$ by solving

$$\hat{\theta}^{k+1} = \arg\min_{\theta \in Q} \sum_{j=0}^{n-1} \hat{w}_j{}^2 [u_j - u(t_j; 10^{\theta})]^2$$

   to obtain the $k+1$ estimate $\hat{\theta}^{k+1}$ for $\hat{\theta}_{gls}$.
4. Set $k = k+1$ and return to Step 2. Terminate when successive estimates for $\hat{\theta}_{gls}$ are sufficiently close, or when one has iterated 20 times. For our problem, our "sufficiently close" criterion was found by determining if $||\hat{\theta}^{k+1} - \hat{\theta}^k||_\infty \leq 10^{-3}$, where $||\theta||_\infty$ is the maximum component of the given vector θ. The parameter values being estimated are all log-scaled, and are thus on the order of $[10^{-1}, 10^1]$. This puts the stopping criterion at two orders of magnitude less than the smallest log-scaled parameter value, which is sufficient in our problem.

Even though we have removed all data points with absolute value under 5×10^{-6}, we still account for the (now unlikely) possibility that some model values may still end up small in absolute value. Thus, we incorporate thresholding on the weights to keep from dividing by zero. We take a weight threshold value of 1×10^{-10}, as this is almost certainly below the threshold of significance in terms of the model displacements. Then, for all indices $\bar{j} \in \{k \mid \; |w_k| < 1 \times 10^{-10}\}$, we set $w_{\bar{j}} = 1 \times 10^{-10}$. This is done each time the weights are re-estimated in Step 2 of the iterative process.

With weight thresholding, we are assured that the iterative process is possible numerically. Thus, similar to the ordinary least squares case, at each step k in the iterative GLS estimation process we are minimizing a continuous function of θ over a compact parameter space Q, and thus the inverse problem in each iteration will have a solution. Also, as long as the iterative process is carried out sufficiently many times, under certain conditions the weights will converge $\hat{w}_j \to u(t_j; 10^{\hat{\theta}_{gls}})^{-1}$ (see, e.g., [16]).

4.2.1 Optimization considerations

As in [8], we used the built-in Matlab routine `lsqnonlin` for our optimization routine to solve for $\hat{\theta}_{ols}$ and $\hat{\theta}_{gls}$. We used the trust-region-reflective (TRR) algorithm that is built in; as our previous effort in [8] demonstrated, the Levenburg-Marquardt option was slower than TRR and did not give us better results. Since we are using at least one relaxation time, we do not consider `fmincon` which we have shown to be ineffective in estimating relaxation times.

In order to start the optimization routines for computing $\hat{\theta}_{ols}$, we must provide initial parameter values (for $\hat{\theta}_{gls}$ we use the estimated value for $\hat{\theta}_{ols}$ as our initial guess). From a perusal of the viscoelastic materials literature, our experience from the previous conceptual work, and from some manual examination on the current data sets, we developed pressure and shear initial values.

Pressure initial guess: For $N_p = 1$, the initial values we use are $E = 4.5 \times 10^4$ Pa, $E_1 = 55$ Pa·s, $\gamma_1 = 1.9 \times 10^5$ Pa, $\tau_1 = 0.05$ s, $A = -1.75 \times 10^{-4}$ m, and $\Upsilon = -0.01$ s. As log-scaled values (c.f. (18)), this gives us

$$\theta^0_{ols} = (4.6532, 1.7404, 5.2788, -1.3010, -3.7570, -2)^T.$$

Shear initial guess: For $N_p = 1$, the values we use are $E = 4.5 \times 10^3$ Pa, $E_1 = 5$ Pa· s, $\gamma_1 = 2.8 \times 10^4$ Pa, $\tau_1 = 0.06$ s, $A = -1.7 \times 10^{-4}$ m, and $\Upsilon = -0.01$ s. As log-scaled values (c.f. (18)), this gives us

$$\theta^0_{gls} = (3.6532, 0.6990, 4.4472, -1.2218, -3.7696, -2)^T.$$

4.2.2 Residuals

We will also include residual plots to assist in analysis of the model fit to data, and to indicate which error model best describes the error in the data. Residuals give a sense for the model fit to data, but more importantly the residuals can give an indication [16] regarding the appropriateness of our error model. If the absolute residuals seem to be randomly dispersed around the horizontal axis and form a horizontal band around that axis, then the absolute error model may be correct. On the other hand, if the (modified) relative residuals seem to be randomly dispersed, then the relative error model may be correct. We define the following:

- **Absolute residuals** are computed as $r_j = u_j - u(t_j; 10^{\hat{\theta}})$, where $\hat{\theta}$ is the particular parameter estimate being considered.

- **Relative residuals** are computed as $r_j = \hat{w_j}(u_j - u(t_j; 10^{\hat{\theta}}))$ where $\hat{w_j} = u(t_j; 10^{\hat{\theta}})^{-1}$ and the $\hat{w_j}$ are thresholded in the same manner as discussed earlier.

4.2.3 Asymptotic error analysis

In addition to determining the parameter estimates $\hat{\theta}_{ols}$ and $\hat{\theta}_{gls}$ for pressure and shear data, we will provide confidence interval information for each entry in the parameter vectors. For the absolute error model, the process is the same as that which we used in [8], and is also described in [16]; for the relative error model, the corresponding asymptotic error methodology is discussed in [16, Ch. 3]. Since the theory is common enough, we do not reiterate it here and refer interested readers to the aforementioned references.

4.3 Results, $N_p = 1$

We now demonstrate the ability of our model to match data. For this purpose, we will take a single relaxation time ($N_p = 1$). We run both the absolute (OLS) and relative (GLS) error models on a sample data set using a 264 g loading weight, separately for both pressure and shear data. We will report parameter estimates, standard errors, plots of model fits to data, plots of residuals versus time, and plots of residuals versus model values. We use these elements in order to recommend error models for the pressure and shear cases.

We will also examine parameter estimation using data sampled at different rates. This will allow for a study of whether the parameter estimates stay consistent as the number of data points is reduced, and will also allow us to examine issues of independence between measurements (data points). It is expected that if the data points are sampled too frequently, nearby measurements are more likely to be dependent. This is due to the inherent limitations in hardware; too frequent sampling may not allow the measurement device to return to its resting state between measurements. Using fewer data points is a way of increasing the likelihood that neighboring measurements are independent. We run the inverse problem on each data set and using each error model with the following two options:

1. Using all the data points (1.024 kHz), and

2. Using every other data point (512 kHz).

Before discussing results, we recall the earlier discussion in Section 4.1 on the sensitivity of model output to the parameters. The pressure model output was most sensitive to E, γ_1, A, and Υ and less sensitive to E_1 and τ_1. The shear model output was most sensitive to G, ζ_1, and A and less sensitive to G_1, τ_1, and Υ. Thus, throughout the results, we are likely to see larger standard errors relative to the parameter magnitude for E_1 (G_1) and τ_1. Intuitively, this is due in part to the fact that in the mathematical model the relaxation times influence how the damping properties of a material are described, and thus there is likely some interplay between the bulk damping parameter E_1 (G_1) and the relaxation time τ_1 in the pressure and shear cases. The parameter Υ is a special case. As discussed in Section 3.1.5, if the relaxation times are small (which they will be in our results) then Υ will not have much of an effect on the model output once it becomes sufficiently negative. Thus, even though the model output is at least somewhat sensitive to Υ, particularly for the pressure model, we may still obtain large confidence intervals for this parameter once sufficiently negative. We will see these larger confidence intervals for Υ in the results, and it should be noted that this is not a major concern since it is an artificial parameter designed to approximate the loading process.

The results of the pressure parameter estimates and confidence intervals (see [5, 6, 8, 10, 16] for information on computing confidence intervals) are shown in Tables 1-4, and the model fits as well as residuals are shown in Figures 6-9. In all cases, model fits to data are good. Comparing the OLS results in Tables 1 and 3 with their GLS counterparts in Tables 2 and 4, we see that the parameter estimates for OLS are generally more consistent between the full and reduced data sets than those for GLS. We also see that the standard errors for OLS are generally smaller than those for GLS for the results using all the data. Even though the OLS standard errors increase slightly when we cut the number of data points used in half, these comparisons give an initial indication that OLS is better than GLS. However, these results are only valid if the error model is correct. To that end, the residuals versus time plots in Figures 6-9 all have some patterns in the residuals but those do not substantially change when going between OLS and GLS. Additionally, these plots show less of a pattern in the residuals (i.e., more random) as the data sampling frequency is reduced. In the same figures, the residuals versus model plots are also not much different when comparing the OLS cases to the GLS cases. From a residual analysis standpoint, then, either model appears reasonable. Thus, since OLS is a simpler error model and since we have a higher degree of confidence in the parameter estimates due to their consistency for different data sampling rates and smaller standard errors, we recommend the OLS model when using pressure data. We do note that the standard error for $\log_{10}(\tau_1)$ for both OLS cases is nearly as large as the parameter estimate itself; this is somewhat expected since the pressure model output is less sensitive to τ_1 as previously discussed. Thus, we do not have as much confidence in the estimate for τ_1 as in the other parameter estimates.

Since there was not a significant difference between OLS and GLS in terms of residual analysis, we examined another error model,

$$U_j = u(t_j; 10^{\theta_0}) + \text{sign}(u(t_j; 10^{\theta_0}))|u(t_j; 10^{\theta_0})|^{1/2}\mathcal{E}_j,$$

which we call the "half error" model (for lack of a better phrase) due to the 1/2 exponent in the final term. This is solved in a manner similar to the "full" GLS, the difference being that here we use the weights $w_j = \left|u(t_j; 10^{\theta})\right|^{-1/2}$. Results of the corresponding inverse problem are shown in in Tables 5-6 and Figures 10-11. There does not appear to be any improvement over the previous OLS and GLS results in terms of residual randomness, and the parameter values are more consistent than those from GLS but less consistent than those from OLS. Additionally, the standard errors when using the half error model are generally larger than those when using OLS. Thus, we continue to conclude that the OLS model is most appropriate for the pressure data.

Shear results are shown in Tables 7-10 and Figures 12-15. In all cases, the model fits to data are good. Comparing the OLS results in Tables 7 and 9 with their GLS counterparts in Tables 8 and 10 we see that the parameter estimates for OLS demonstrate similar consistency when using the full and reduced data sets as the GLS estimates. The standard errors for the GLS cases are larger than the OLS cases. In Figures 12-15, the residuals versus model plots are again not noticeably different for the OLS and GLS cases. The initial indication is that we have more confidence in the OLS results. However, the time versus residual plots raise cause for concern. In the OLS residual versus time plots, there is a noticeable "fan" structure for early times. However, for the GLS error model, the residual versus time plots do not show a fan structure and are fairly randomly distributed. Since this indicates that the OLS error model may not be correct, we are inclined to recommend the GLS error model in the shear case so that we do not mistakenly overstate our confidence in the parameter estimates, which we could do if we used the parameter estimates from the possibly-wrong OLS case.

Pressure parameter estimates, standard errors (SE), and 95% confidence intervals (CI95):

Table 1: Pressure optimization results and confidence analysis for OLS on a 264 g data set using every data point.

Param.	Estimate	SE	CI95
$\log_{10}(E)$	4.6164	0.5071	(3.6140, 5.6188)
$\log_{10}(E_1)$	1.7385	0.2180	(1.3076, 2.1694)
$\log_{10}(\tau_1)$	-1.3365	0.5089	(-2.3425, -0.3306)
$\log_{10}(\gamma_1)$	5.2748	0.1096	(5.0581, 5.4914)
$\log_{10}(-A)$	-3.7520	0.0061	(-3.7641, -3.7399)
$\log_{10}(-\Upsilon)$	-1.8549	0.6463	(-3.1326, -0.5773)

Young's modulus dynamic analog $E_0 = 229.604$ kPa (static $E_0 = 213.239$ kPa)

Table 2: Pressure optimization results and confidence analysis for GLS on a 264 g data set using every data point.

Param.	Estimate	SE	CI95
$\log_{10}(E)$	5.0523	2.1445	(0.8131, 9.2915)
$\log_{10}(E_1)$	1.8025	0.2192	(1.3692, 2.2358)
$\log_{10}(\tau_1)$	-0.7878	2.1350	(-5.0082, 3.4326)
$\log_{10}(\gamma_1)$	5.0664	2.0697	(0.9750, 9.1578)
$\log_{10}(-A)$	-3.8031	0.0124	(-3.8276, -3.7786)
$\log_{10}(-\Upsilon)$	-1.0152	4.9889	(-10.8772, 8.8468)

Young's modulus dynamic analog $E_0 = 229.323$ kPa (static $E_0 = 213.239$ kPa)

Table 3: Pressure optimization results and confidence analysis for OLS on a 264 g data set using every other data point.

Param.	Estimate	SE	CI95
$\log_{10}(E)$	4.6051	0.8396	(2.9302, 6.2800)
$\log_{10}(E_1)$	1.7426	0.3850	(0.9745, 2.5107)
$\log_{10}(\tau_1)$	-1.3661	0.8407	(-3.0433, 0.3111)
$\log_{10}(\gamma_1)$	5.2775	0.1755	(4.9274, 5.6277)
$\log_{10}(-A)$	-3.7442	0.0080	(-3.7601, -3.7284)
$\log_{10}(-\Upsilon)$	-1.8921	1.0604	(-4.0075, 0.2233)

Young's modulus dynamic analog $E_0 = 229.749$ kPa (static $E_0 = 213.239$ kPa)

Table 4: Pressure optimization results and confidence analysis for GLS on a 264 g data set using every other data point.

Param.	Estimate	SE	CI95
$\log_{10}(E)$	4.1586	0.1827	(3.7942, 4.5231)
$\log_{10}(E_1)$	1.2236	0.4868	(0.2525, 2.1948)
$\log_{10}(\tau_1)$	-1.6888	0.1550	(-1.9981, -1.3794)
$\log_{10}(\gamma_1)$	5.3313	0.0134	(5.3045, 5.3580)
$\log_{10}(-A)$	-3.8057	0.0169	(-3.8393, -3.7721)
$\log_{10}(-\Upsilon)$	-2.2436	0.1726	(-2.5879, -1.8992)

Young's modulus dynamic analog $E_0 = 228.827$ kPa (static $E_0 = 213.239$ kPa)

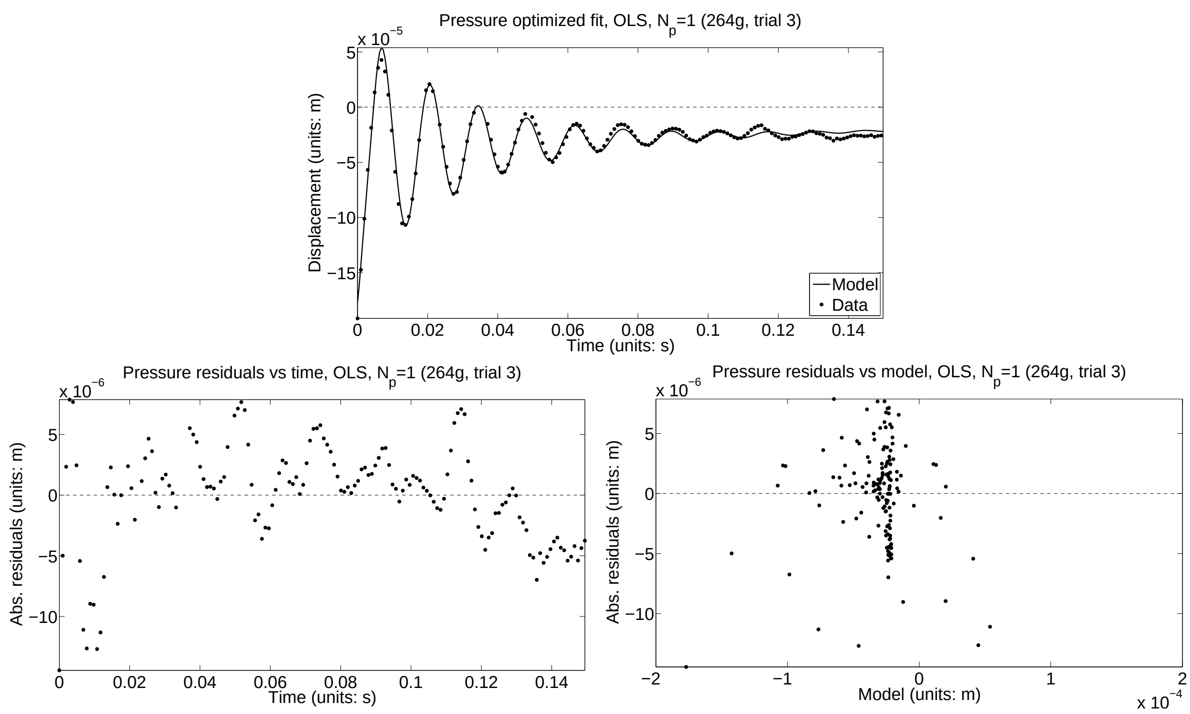

Figure 6: Pressure data fit using every data point with absolute error model, $N_p = 1$, weight 264 g. (top) Model fit to data. (bottom left) Absolute residuals vs time. (bottom right) Absolute residuals vs model.

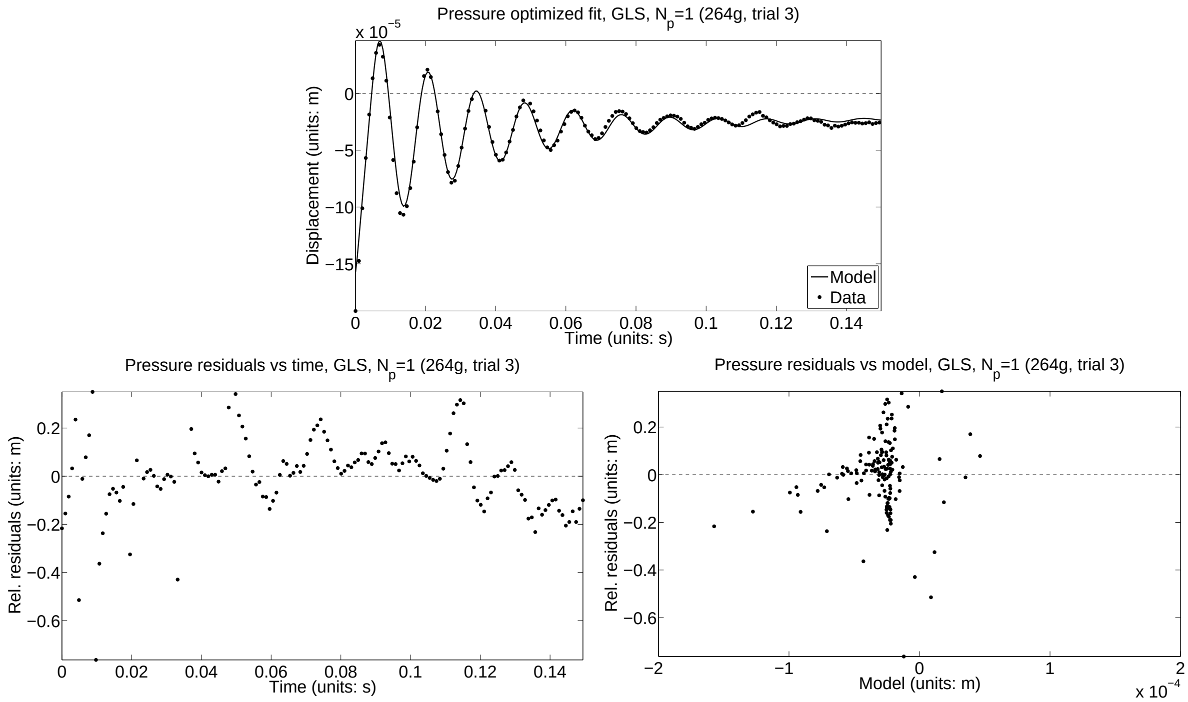

Figure 7: Pressure data fit using every data point with relative error model, $N_p = 1$, weight 264 g. (top) Model fit to data. (bottom left) Relative residuals vs time. (bottom right) Relative residuals vs model.

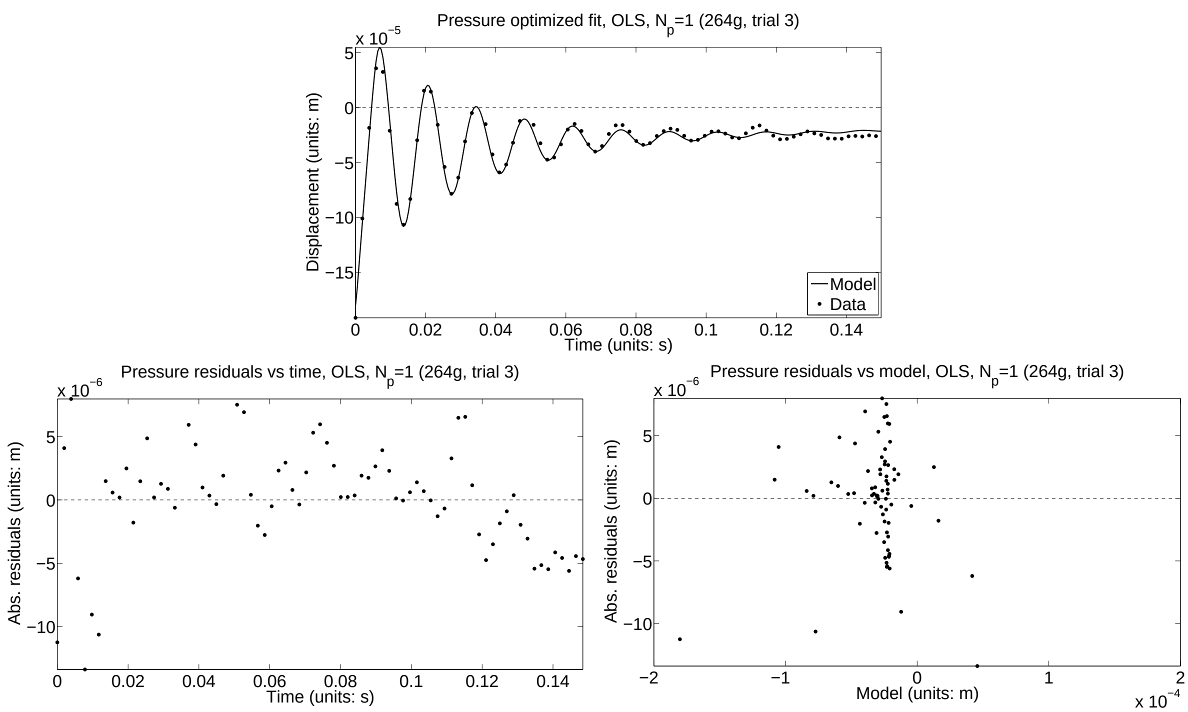

Figure 8: Pressure data fit using every other data point with absolute error model, $N_p = 1$, weight 264 g. (top) Model fit to data. (bottom left) Absolute residuals vs time. (bottom right) Absolute residuals vs model.

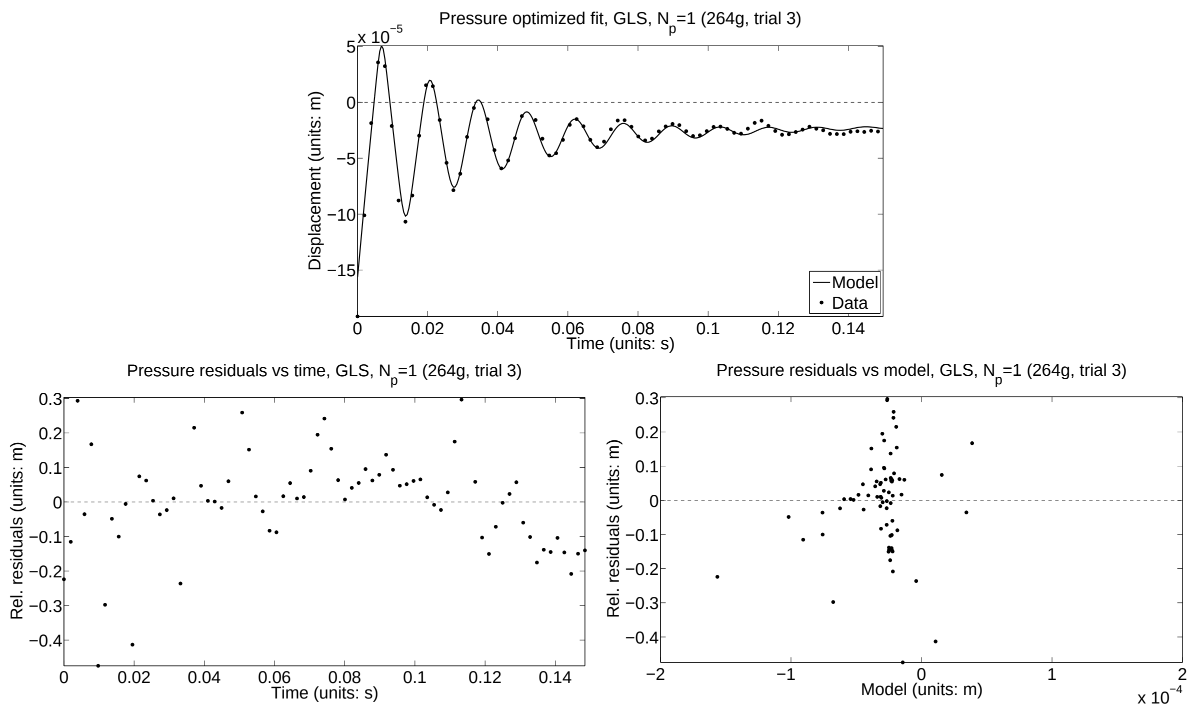

Figure 9: Pressure data fit using every other data point with relative error model, $N_p = 1$, weight 264 g. (top) Model fit to data. (bottom left) Relative residuals vs time. (bottom right) Relative residuals vs model.

Table 5: Pressure optimization results and confidence analysis for GLS (half error) on a 264 g data set, using every data point.

Param.	Estimate	SE	CI95
$\log_{10}(E)$	4.7747	0.9355	(2.9254, 6.6240)
$\log_{10}(E_1)$	1.7594	0.2289	(1.3069, 2.2120)
$\log_{10}(\tau_1)$	-1.1169	0.9304	(-2.9562, 0.7223)
$\log_{10}(\gamma_1)$	5.2302	0.3247	(4.5883, 5.8721)
$\log_{10}(-A)$	-3.7831	0.0091	(-3.8011, -3.7651)
$\log_{10}(-\Upsilon)$	-1.5638	1.3384	(-4.2095, 1.0818)

Young's modulus dynamic analog $E_0 = 229.421$ kPa (static $E_0 = 213.239$ kPa)

Table 6: Pressure optimization results and confidence analysis for GLS (half error) on a 264 g data set, using every other data point.

Param.	Estimate	SE	CI95
$\log_{10}(E)$	4.5630	0.9095	(2.7486, 6.3774)
$\log_{10}(E_1)$	1.6866	0.4513	(0.7863, 2.5869)
$\log_{10}(\tau_1)$	-1.3489	0.9004	(-3.1452, 0.4473)
$\log_{10}(\gamma_1)$	5.2848	0.1699	(4.9458, 5.6238)
$\log_{10}(-A)$	-3.7797	0.0128	(-3.8052, -3.7542)
$\log_{10}(-\Upsilon)$	-1.8602	1.1158	(-4.0862, 0.3657)

Young's modulus dynamic analog $E_0 = 229.224$ kPa (static $E_0 = 213.239$ kPa)

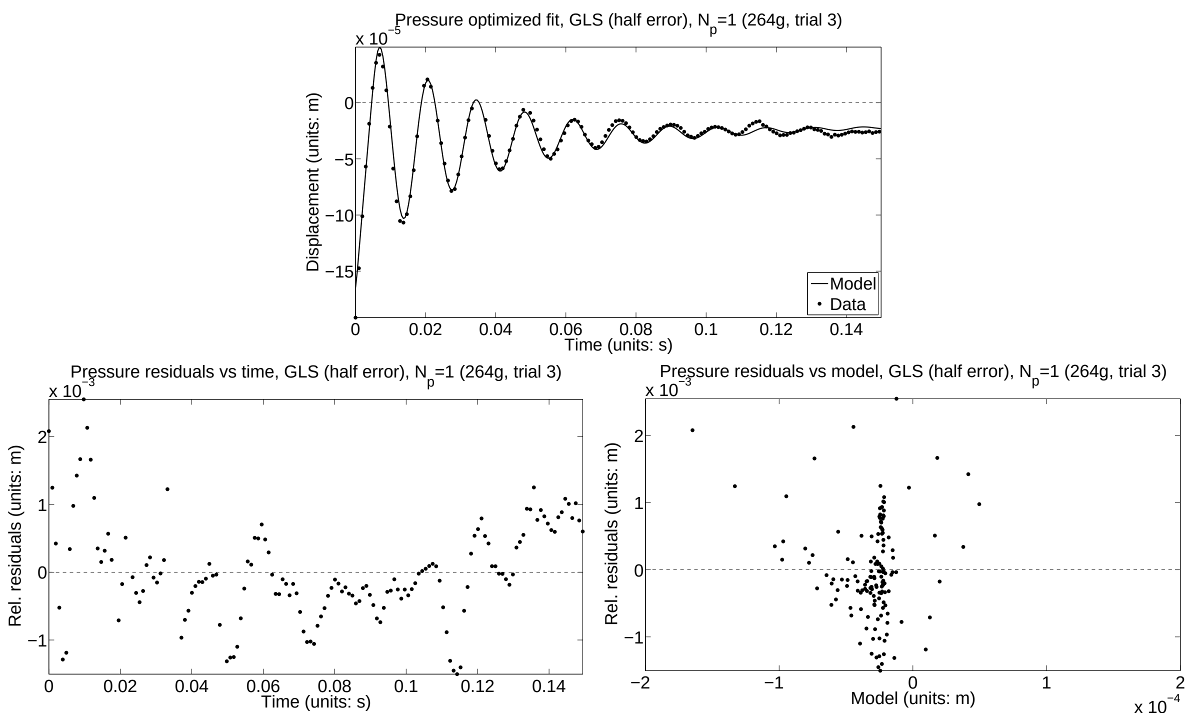

Figure 10: Pressure data fit using every data point with relative half error model, $N_p = 1$, weight 264 g. (top) Model fit to data. (bottom left) Relative residuals vs time. (bottom right) Relative residuals vs model.

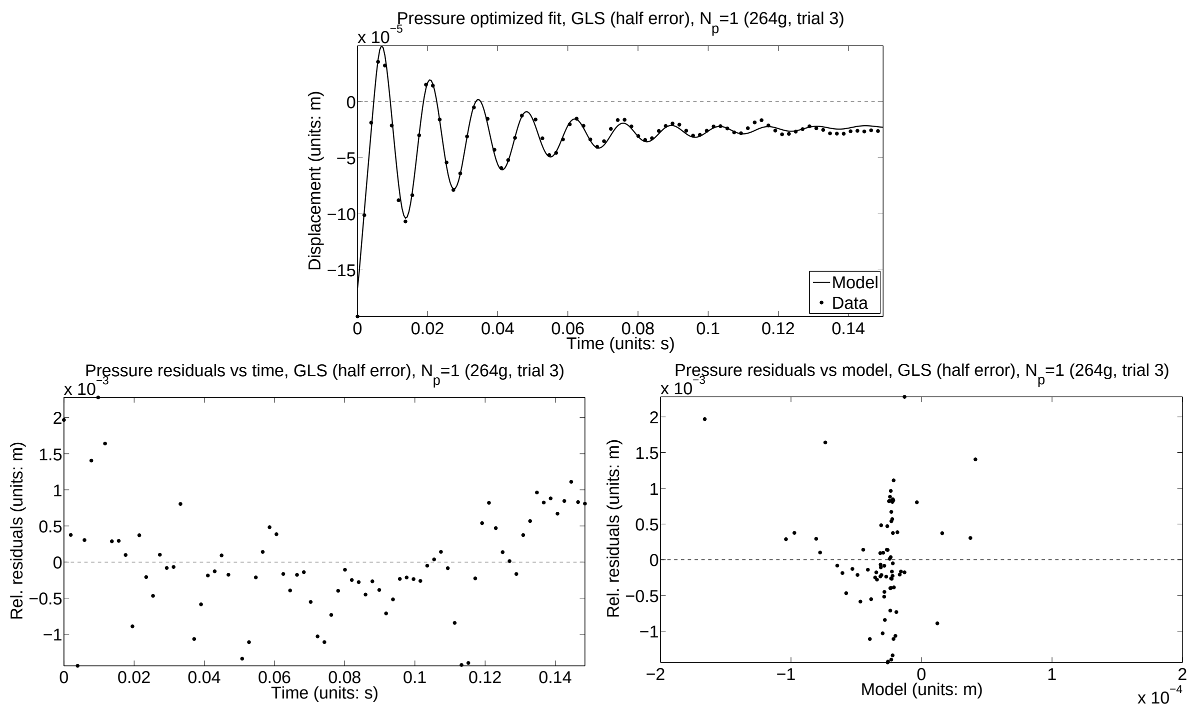

Figure 11: Pressure data fit using every other data point with relative half error model, $N_p = 1$, weight 264 g. (top) Model fit to data. (bottom left) Relative residuals vs time. (bottom right) Relative residuals vs model.

Shear parameter estimates, standard errors (SE), and 95% confidence intervals (CI95):

Table 7: Shear optimization results and confidence analysis for OLS on a 264 g data set using every data point.

Param.	Estimate	SE	CI95
$\log_{10}(G)$	3.6362	0.2465	(3.1499, 4.1225)
$\log_{10}(G_1)$	0.4725	0.2025	(0.0730, 0.8719)
$\log_{10}(\tau_1)$	-1.3433	0.2455	(-1.8276, -0.8589)
$\log_{10}(\zeta_1)$	4.4637	0.0366	(4.3915, 4.5358)
$\log_{10}(-A)$	-3.7543	0.0054	(-3.7649, -3.7436)
$\log_{10}(-\Upsilon)$	-2.0632	0.2862	(-2.6278, -1.4985)

Shear modulus dynamic analog $G_0 = 33.411$ kPa (static $G_0 = 123.289$ kPa)

Table 8: Shear optimization results and confidence analysis for GLS on a 264 g data set using every data point.

Param.	Estimate	SE	CI95
$\log_{10}(G)$	4.1059	1.0993	(1.9371, 6.2747)
$\log_{10}(G_1)$	0.5925	0.2149	(0.1686, 1.0165)
$\log_{10}(\tau_1)$	-0.8318	1.1018	(-3.0054, 1.3418)
$\log_{10}(\zeta_1)$	4.3150	0.6781	(2.9774, 5.6527)
$\log_{10}(-A)$	-3.7990	0.0093	(-3.8173, -3.7807)
$\log_{10}(-\Upsilon)$	-1.3449	1.8982	(-5.0898, 2.4000)

Shear modulus dynamic analog $G_0 = 33.416$ kPa (static $G_0 = 123.289$ kPa)

Table 9: Shear optimization results and confidence analysis for OLS on a 264 g data set using every other data point.

Param.	Estimate	SE	CI95
$\log_{10}(G)$	3.5431	0.2498	(3.0469, 4.0393)
$\log_{10}(G_1)$	0.3753	0.3227	(-0.2657, 1.0164)
$\log_{10}(\tau_1)$	-1.4450	0.2474	(-1.9364, -0.9535)
$\log_{10}(\zeta_1)$	4.4761	0.0294	(4.4178, 4.5345)
$\log_{10}(-A)$	-3.7501	0.0071	(-3.7643, -3.7360)
$\log_{10}(-\Upsilon)$	-2.1813	0.2779	(-2.7334, -1.6293)

Shear modulus dynamic analog $G_0 = 33.423$ kPa (static $G_0 = 123.289$ kPa)

Table 10: Shear optimization results and confidence analysis for GLS on a 264 g data set using every other data point.

Param.	Estimate	SE	CI95
$\log_{10}(G)$	3.8649	1.0435	(1.7922, 5.9377)
$\log_{10}(G_1)$	0.5449	0.3561	(-0.1625, 1.2523)
$\log_{10}(\tau_1)$	-1.0217	1.0543	(-3.1161, 1.0726)
$\log_{10}(\zeta_1)$	4.4171	0.2918	(3.8375, 4.9967)
$\log_{10}(-A)$	-3.8026	0.0119	(-3.8263, -3.7789)
$\log_{10}(-\Upsilon)$	-1.6729	1.3806	(-4.4153, 1.0695)

Shear modulus dynamic analog $G_0 = 33.454$ kPa (static $G_0 = 123.289$ kPa)

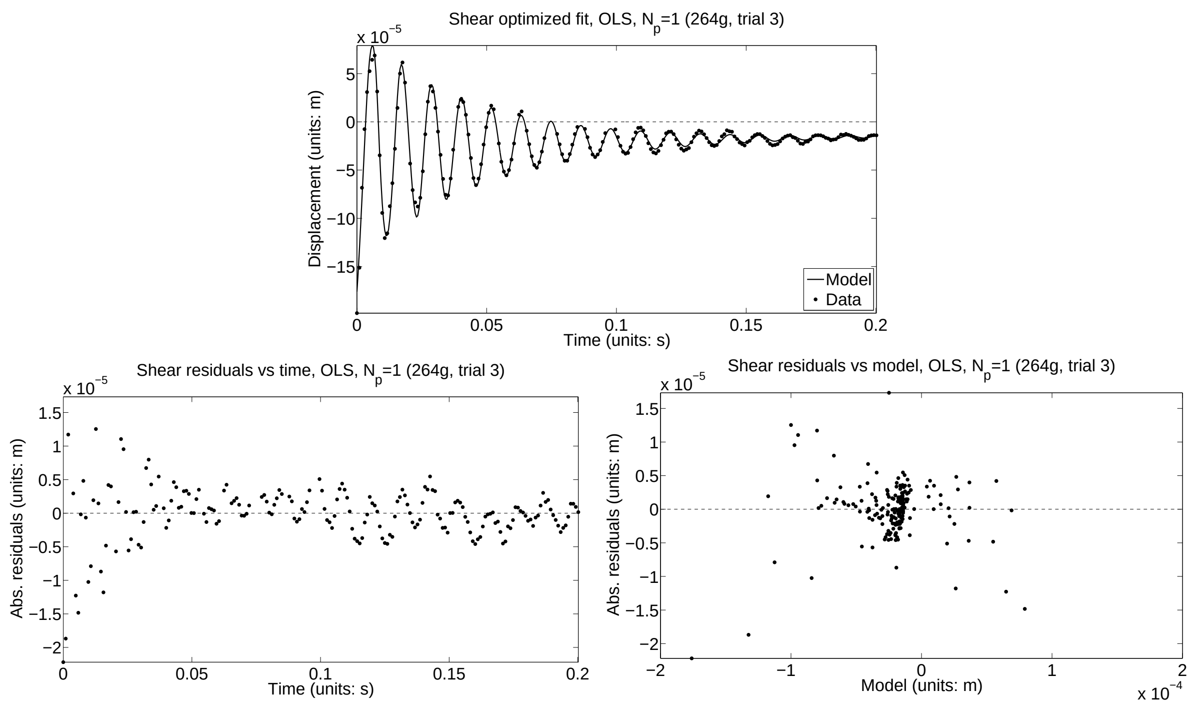

Figure 12: Shear data fit using every data point with absolute error model, $N_p = 1$, weight 264 g. (top) Model fit to data. (bottom left) Absolute residuals vs time. (bottom right) Absolute residuals vs model.

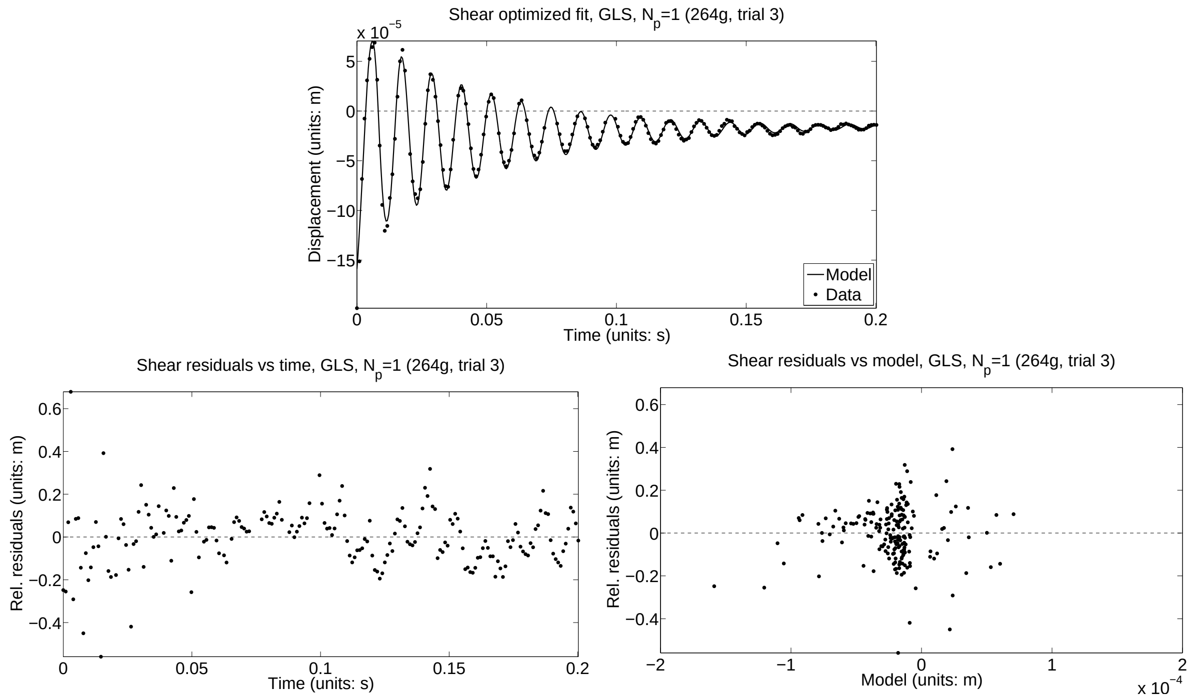

Figure 13: Shear data fit using every data point with relative error model, $N_p = 1$, weight 264 g. (top) Model fit to data. (bottom left) Relative residuals vs time. (bottom right) Relative residuals vs model.

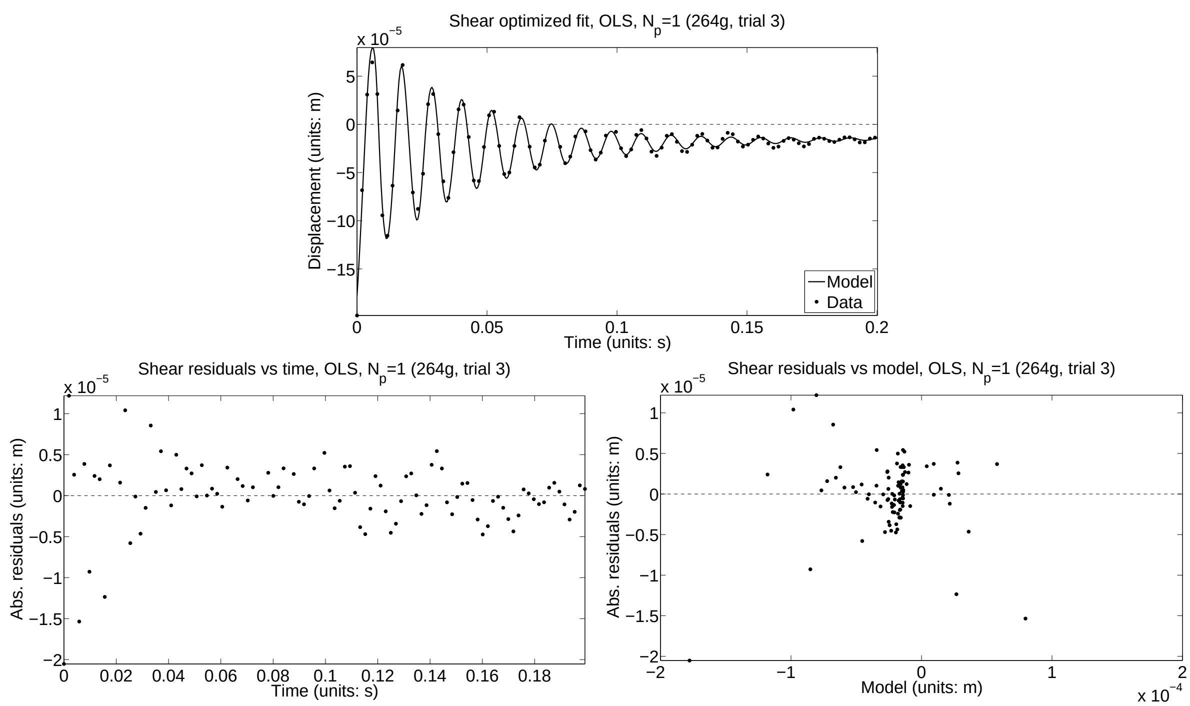

Figure 14: Shear data fit using every other data point with absolute error model, $N_p = 1$, weight 264 g. (top) Model fit to data. (bottom left) Absolute residuals vs time. (bottom right) Absolute residuals vs model.

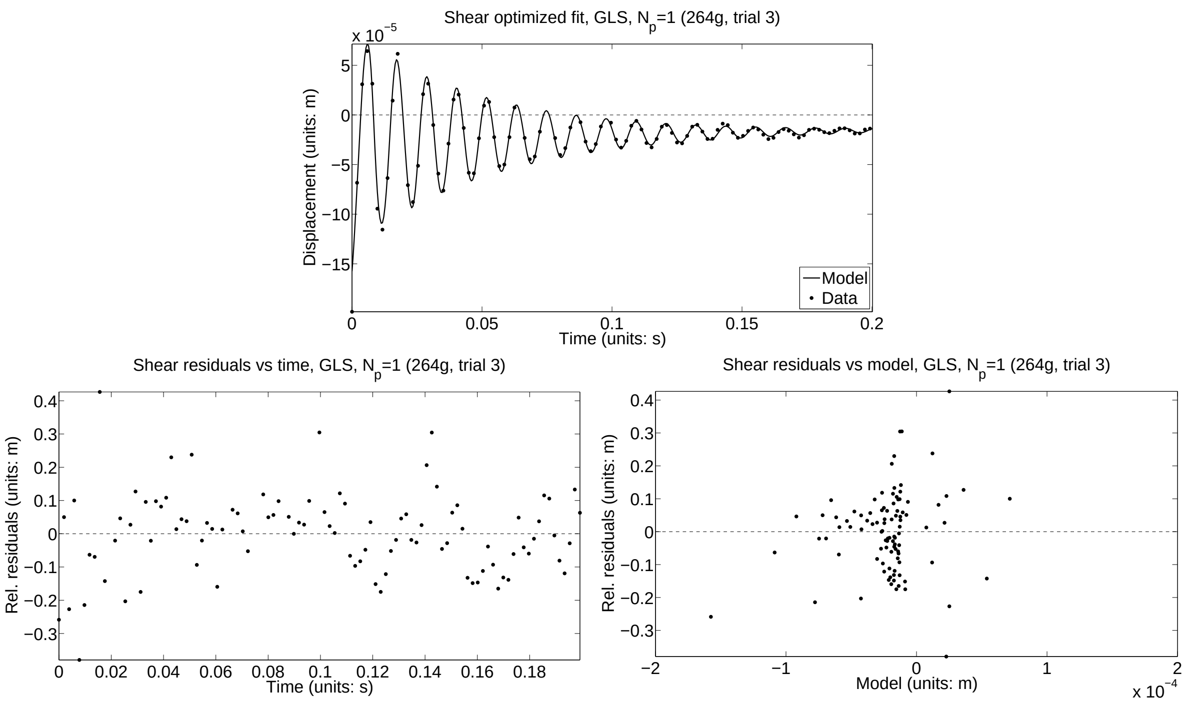

Figure 15: Shear data fit using every other data point with relative error model, $N_p = 1$, weight 264 g. (top) Model fit to data. (bottom left) Relative residuals vs time. (bottom right) Relative residuals vs model.

5 Discussion and Future Work

We have developed an updated one-dimensional viscoelastic model for tissue and have used experimental data from a simple homogeneous gel phantom to test the ability of our model to describe wave propagation in the medium. The data were generated from a drop experiment designed to mimic the disturbance into the chest cavity produced by blood flow in a stenosed coronary artery impacting the vessel wall, a disturbance which results in pressure and shear waves propagating away from the vessel walls downstream of the blockage. In our inverse problem results as discussed in Section 4.3, we have shown an ability to consistently model the wave propagation using different error models and at different data frequencies, obtaining good fits to data in all of our inverse problems. In addition to a good fit, though, we also examined statistical properties of the parameter estimators as well as residual plots to gain more insight into the proper error model for the pressure and shear data sets. This is necessary, since a correct error model is essential in order to apply the asymptotic error theory properly and thus obtain correct confidence intervals. For the pressure case, we prefer the absolute error model (OLS) over the relative error model (GLS) since the residual plots indicated no noticeable difference between the two models while the OLS parameter estimates were more consistent and had generally smaller corresponding standard errors. For the shear case, we recommend taking the more conservative route and using the GLS parameter estimates; even though the GLS estimates had larger standard errors, there were indications from the residual versus time plots for OLS that the OLS model is not correct.

In the future, we may try to estimate more than one relaxation time. Initial attempts indicated some difficulty, as the optimization algorithms tended toward parameter values which caused the model to damp out quickly and go through the mean of the data oscillations. Ongoing examinations indicate that we can overcome this by providing constraints on some of the parameters, particularly τ_j and $E_1(G_1)$. This may also be due to the previously discussed fact that data points too near zero cause problems when computing relative residuals, so we will examine the same data thresholding method as was discussed earlier.

We are currently examining a two dimensional model and corresponding experimental configurations. Experiments are currently in progress to produce a two dimensional wave from different points in the medium and with different detection points along the outer wall of the phantom. It is conceivable that the one dimensional parameters could be used as a rough first approximation in a corresponding two dimensional code, which would allow us to focus on trying to determine the location of the wave generation in the medium. Also, these parameter values could be used in a model of wave propagation in another conceptual device designed to mimic a constricted artery and the waves that result from passing fluid through a constricted pipe in the center of the medium.

In the slightly longer term, we will also likely need to conduct an inverse problem using a two dimensional model and corresponding data. These one dimensional results will provide a starting point for parameters in that inverse problem, hopefully decreasing runtime and the time it takes to find viable parameters. The same issues discussed here (sensitivity to parameters, data frequency, number of relaxation times) will again be of concern for the two dimensional problem. Future efforts will also involve scaling up all these experiments to larger phantoms and then to some sort of actual tissue sample experiments.

Overall, we have successfully demonstrated the ability of the pressure and shear mathematical models to accurately describe the data from laboratory experiments. A linear viscoelastic constitutive relationship, i.e., (16b) and (17b), was adequate. This is a significant achievement, as all the work previously discussed was limited to inverse problems on simulated data or data that was not from the impulse-type experiments.

6 Acknowledgements

This research was supported in part (HTB,SH,ZRK) by Grant Number R01AI071915-09 from the National Institute of Allergy and Infectious Diseases, in part (HTB,SH,ZRK) by the Air Force Office of Scientific Research under grant number AFOSR FA9550-12-1-0188, in part (ZRK) by the Department of Education with a GAANN Fellowship under grant number P200A070386, in part (CK,SS,JW) by the Engineering and Physical Sciences Research Council EP/H011072/1, and in part (MBr,SG,MBi) by the Engineering and Physical Sciences Research Council EP/H011285/1.

References

[1] M. Akay, Noninvasive detection of coronary artery disease using advanced signal processing methods, PhD. Dissertation, Rutgers University, Piscataway, NJ, 1990.

[2] H.T. Banks, *A Functional Analysis Framework for Modeling, Estimation and Control in Science and Engineering*, CRC Press, Boca Raton London New York, 2012.

[3] H.T. Banks, J.H. Barnes, A. Eberhardt, H. Tran, and S. Wynne, Modeling and computation of propagating waves from coronary stenoses, *Computation and Applied Mathematics*, **21** (2002), 767–788.

[4] H.T. Banks and K. Bihari, Modelling and estimating uncertainty in parameter estimation, *Inverse Problems*, **17** (2001), 95–111.

[5] H.T. Banks and B.G. Fitzpatrick, Inverse problems for distributed systems: statistical tests and ANOVA, LCDS/CCS Rep. 88-16, July, 1988, Brown University; *Proc. International Symposium on Math. Approaches to Envir. and Ecol. Problems*, Springer Lecture Notes in Biomath., **81** (1989), 262–273.

[6] H.T. Banks, K. Holm and D. Robbins, Standard error computations for uncertainty quantification in inverse problems: Asymptotic theory vs. Bootstrapping, CRSC-TR09-13, N.C. State University, June 2009; Revised May 2010; *Mathematical and Computer Modelling*, **52** (2010), 1610–1625.

[7] H.T. Banks, S. Hu, Z.R. Kenz, A brief review of elasticity and viscoelasticity for solids, *Advances in Applied Mathematics and Mechanics*, **3** (2011), 1–51.

[8] H.T. Banks, S. Hu, Z.R. Kenz, C. Kruse, S. Shaw, J.R. Whiteman, M.P. Brewin, S.E. Greenwald and M.J. Birch, Material parameter estimation and hypothesis testing on a 1D viscoelastic stenosis model: Methodology, CRSC-TR12-09, N.C. State University, April 2012; *J. Inverse and Ill-Posed Problems*, to appear, 34 pages; DOI 10.1515/jip-2012-0081.

[9] H.T. Banks, Z.R. Kenz and W.C. Thompson, A review of selected techniques in inverse problem nonparametric probability distribution estimation, *J. of Inverse and Ill-Posed Problems*, **20** (2012), 429–460; DOI 10.1515/jip-2012-0037.

[10] H.T. Banks, Z.R. Kenz and W.C. Thompson, An extension of RSS-based model comparison tests for weighted least squares, CRSC-TR12-18, N. C. State University, Raleigh, NC, August, 2012; *Intl. J. Pure and Appl. Math.,* **79** (2012), 155–183.

[11] H.T. Banks and N. Luke, Modeling of propagating shear waves in biotissue employing an internal variable approach to dissipation, *Communication in Computational Physics*, **3** (2008), 603–640.

[12] H.T. Banks, N. Medhin, and G. Pinter, Multiscale considerations in modeling of nonlinear elastomers, *International Journal for Computational Methods in Engineering Science and Mechanics*, **8** (2007), 53–62.

[13] H.T. Banks, N. Medhin, and G. Pinter, Nonlinear reptation in molecular based hysteresis models for polymers, *Quarterly of Applied Math.*, **62** (2004), 767–779.

[14] H.T. Banks and G.A. Pinter, A probabilistic multiscale approach to hysteresis in shear wave propagation in biotissue, *Multiscale Modeling and Simulation*, **3** (2005), 395–412.

[15] H.T. Banks and J.R. Samuels, Jr, Detection of cardiac occlusions using viscoelastic wave propagation, *Advances in Applied Mathematics and Mechanics*, **1** (2009), 1–28.

[16] H.T. Banks and H.T. Tran, *Mathematical and Experimental Modeling of Physical and Biological Processes*, CRC Press, Boca Raton, FL, 2009.

[17] M.P. Brewin, M.J. Birch, S.E. Greenwald, et. al., Characterization of the uniaxial elastic properties of an agar-based tissue mimicking material, *in preparation*.

[18] C. Kruse, S. Shaw, J.R. Whiteman, et. al., High order space-time finite element schemes for acoustic and viscodynamic wave equations with temporal decoupling, *in preparation*.

[19] N. Luke, Modeling shear wave propagation in biotissue: An internal variable approach to dissipation, PhD Thesis, N.C. State University, Raleigh, 2006.

[20] N. Owsley and A. Hull, Beamformed nearfield imaging of a simulated coronary artery containing a stenosis, *IEEE Trans. Med. Imaging*, **17** (1998), 900–909.

[21] N. Owsley, A.J. Hull, M.H. Ahmed, and J. Kassal, A proof of concept experiment for the detection of occluded coronary arteries using array sensor technology, *Engr. in Medicine and Biol. Society*, IEEE 17th Annual Conf., **1** (1995), 145–146.

[22] J. R. Samuels, Jr. Inverse problems and post analysis techniques for a stenosis-driven acoustic wave propagation model, PhD Thesis, N.C. State University, Raleigh, 2008.

[23] J. Semmlow and K. Rahalkar, Acoustic detection of coronary artery disease, *Annu. Rev. Biomed. Eng*, **9** (2007), 449–469.

[24] J. Verburg and E. van Vollenhoven, Phonocardiography: Pysical and technical aspect and clinical uses, in *Noninvasive Physiological Measurements* (ed. P. Rolfe), Academic Press, London, 1979, p. 213–259.

[25] J. Wloka, *Partial Differential Equations*, Cambridge University Press, Cambridge, 1987.

A Sensitivity Equations

A.1 Pressure Model

1. Sensitivity PDE for ρ (where $s^\rho = \dfrac{\partial u}{\partial \rho}$):

$$\begin{aligned} &\rho(s^\rho)_{tt} - (\sigma_\rho)_x = -u_{tt} \\ &s^\rho(0,t) = 0, \quad \sigma_\rho(L,t) = 0, \\ &s^\rho(x,0) = 0, \quad (s^\rho)_t(x,0) = 0, \end{aligned} \tag{A.1a}$$

In the above equation, the sensitivity of stress with respect to ρ (i.e., σ_ρ) is given by

$$\sigma_\rho \quad = \quad E_1(s^\rho)_{xt} + \left(E + \sum_{j=1}^{N_p} \gamma_j\right)(s^\rho)_x - \sum_{j=1}^{N_p} \gamma_j \epsilon^j_\rho. \tag{A.1b}$$

The sensitivity of the internal variabl ϵ^j with respect to ρ (i.e., $\epsilon^j_\rho = \dfrac{\partial \epsilon^j}{\partial \rho}$) satisfies (for $j = 1, \ldots, N_p$).

$$\tau_j(\epsilon^j_\rho)_t + \epsilon^j_\rho = (s^\rho)_x, \quad \epsilon^j_\rho(0) = 0. \tag{A.1c}$$

2. Sensitivity PDE for E (where $s^E = \dfrac{\partial u}{\partial E}$):

$$\begin{aligned} &\rho(s^E)_{tt} - (\sigma_E)_x = 0 \\ &s^E(0,t) = 0, \quad \sigma_E(L,t) = 0, \\ &s^E(x,0) = 0, \quad (s^E)_t(x,0) = 0, \end{aligned} \tag{A.2a}$$

In the above equation, the sensitivity of stress with respect to E (i.e., σ_E) is given by

$$\sigma_E \quad = \quad E_1(s^E)_{xt} + \left(E + \sum_{j=1}^{N_p} \gamma_j\right)(s^E)_x - \sum_{j=1}^{N_p} \gamma_j \epsilon^j_E + u_x. \tag{A.2b}$$

The sensitivity of the internal variabl ϵ^j with respect to E (i.e., $\epsilon^j_E = \dfrac{\partial \epsilon^j}{\partial E}$) satisfies, for $j = 1, \ldots, N_p$,

$$\tau_j(\epsilon^j_E)_t + \epsilon^j_E = (s^E)_x, \quad \epsilon^j_E(0) = 0. \tag{A.2c}$$

3. Sensitivity PDE for E_1 (where $s^{E_1} = \dfrac{\partial u}{\partial E_1}$):

$$\begin{aligned} &\rho(s^{E_1})_{tt} - (\sigma_{E_1})_x = 0 \\ &s^{E_1}(0,t) = 0, \quad \sigma_{E_1}(L,t) = 0, \\ &s^{E_1}(x,0) = 0, \quad (s^{E_1})_t(x,0) = 0, \end{aligned} \tag{A.3a}$$

In the above equation, the sensitivity of stress with respect to E_1 (i.e., σ_{E_1}) is given by

$$\sigma_{E_1} \quad = \quad E_1(s^{E_1})_{xt} + \left(E + \sum_{j=1}^{N_p} \gamma_j\right)(s^{E_1})_x - \sum_{j=1}^{N_p} \gamma_j \epsilon^j_{E_1} + u_{xt}. \tag{A.3b}$$

The sensitivity of the internal variabl ϵ^j with respect to E_1 (i.e., $\epsilon^j_{E_1} = \dfrac{\partial \epsilon^j}{\partial E_1}$) satisfies, for $j = 1, \ldots, N_p$,

$$\tau_j(\epsilon^j_{E_1})_t + \epsilon^j_{E_1} = (s^{E_1})_x, \quad \epsilon^j_{E_1}(0) = 0. \tag{A.3c}$$

4. Sensitivity PDE for τ_k (where $s^{\tau_k} = \dfrac{\partial u}{\partial \tau_k}$):

$$
\begin{aligned}
&\rho (s^{\tau_k})_{tt} - (\sigma_{\tau_k})_x = 0 \\
&s^{\tau_k}(0,t) = 0, \quad \sigma_{\tau_k}(L,t) = \frac{A}{L}\gamma_k \left(\frac{t}{\tau_k^2} e^{-t/\tau_k} - \frac{t-\Upsilon}{\tau_k^2} e^{-(t-\Upsilon)/\tau_k} \right), \\
&s^{\tau_k}(x,0) = 0, \quad (s^{\tau_k})_t(x,0) = 0,
\end{aligned} \tag{A.4a}
$$

In the above equation, the sensitivity of stress with respect to τ_k (i.e., σ_{τ_k}) is given by

$$
\sigma_{\tau_k} = E_1 (s^{\tau_k})_{xt} + \left(E + \sum_{j=1}^{N_p} \gamma_j \right) (s^{\tau_k})_x - \sum_{j=1}^{N_p} \gamma_j \epsilon^j_{\tau_k}. \tag{A.4b}
$$

The sensitivity of the internal variabl ϵ^j with respect to τ_k (i.e., $\epsilon^j_{\tau_k} = \dfrac{\partial \epsilon^j}{\partial \tau_k}$) satisfies, for $j = 1, \ldots, N_p$,

- if $j = k$ then

$$
\tau_k (\epsilon^k_{\tau_k})_t + \epsilon^k_{\tau_k} = (s^{\tau_k})_x - \epsilon^k_t, \quad \epsilon^k_{\tau_k}(0) = 0, \tag{A.4c}
$$

- if $j \neq k$ then

$$
\tau_j (\epsilon^j_{\tau_k})_t + \epsilon^j_{\tau_k} = (s^{\tau_k})_x, \quad \epsilon^j_{\tau_k}(0) = 0. \tag{A.4d}
$$

5. Sensitivity PDE for γ_k (where $s^{\gamma_k} = \dfrac{\partial u}{\partial \gamma_k}$):

$$
\begin{aligned}
&\rho (s^{\gamma_k})_{tt} - (\sigma_{\gamma_k})_x = 0 \\
&s^{\gamma_k}(0,t) = 0, \quad \sigma_{\gamma_k}(L,t) = \frac{A}{L} \left(e^{-t/\tau_k} - e^{-(t-\Upsilon)/\tau_k} \right), \\
&s^{\gamma_k}(x,0) = 0, \quad (s^{\gamma_k})_t(x,0) = 0,
\end{aligned} \tag{A.5a}
$$

In the above equation, the sensitivity of stress with respect to γ_k (i.e., σ_{γ_k}) is given by

$$
\sigma_{\gamma_k} = E_1 (s^{\gamma_k})_{xt} + \left(E + \sum_{j=1}^{N_p} \gamma_j \right) (s^{\gamma_k})_x - \sum_{j=1}^{N_p} \gamma_j \epsilon^j_{\gamma_k} + u_x - \epsilon^k. \tag{A.5b}
$$

The sensitivity of the internal variabl ϵ^j with respect to γ_k (i.e., $\epsilon^j_{\gamma_k} = \dfrac{\partial \epsilon^j}{\partial \gamma_k}$) satisfies, for $j = 1, \ldots, N_p$,

$$
\tau_j (\epsilon^j_{\gamma_k})_t + \epsilon^j_{\gamma_k} = (s^{\gamma_k})_x, \quad \epsilon^j_{\gamma_k}(0) = 0. \tag{A.5c}
$$

6. Sensitivity PDE for A (where $s^A = \dfrac{\partial u}{\partial A}$):

$$
\begin{aligned}
&\rho (s^A)_{tt} - (\sigma_A)_x = 0 \\
&s^A(0,t) = 0, \quad \sigma_A(L,t) = \frac{1}{L} \left(\sum_{j=1}^{N_p} \gamma_j e^{-t/\tau_j} - \sum_{j=1}^{N_p} \gamma_j e^{-(t-\Upsilon)/\tau_j} \right), \\
&s^A(x,0) = x/L, \quad (s^A)_t(x,0) = 0,
\end{aligned} \tag{A.6a}
$$

In the above equation, the sensitivity of stress with respect to A (i.e., σ_A) is given by

$$
\sigma_A = E_1 (s^A)_{xt} + \left(E + \sum_{j=1}^{N_p} \gamma_j \right) (s^A)_x - \sum_{j=1}^{N_p} \gamma_j \epsilon^j_A. \tag{A.6b}
$$

The sensitivity of the internal variabl ϵ^j with respect to A (i.e., $\epsilon^j_A = \dfrac{\partial \epsilon^j}{\partial A}$) satisfies, for $j = 1, \ldots, N_p$,

$$
\tau_j (\epsilon^j_A)_t + \epsilon^j_A = (s^A)_x, \quad \epsilon^j_A(0) = 0. \tag{A.6c}
$$

7. Sensitivity PDE for Υ (where $s^{\Upsilon} = \dfrac{\partial u}{\partial \Upsilon}$):

$$\begin{aligned} &\rho(s^{\Upsilon})_{tt} - (\sigma_{\Upsilon})_x = 0 \\ &s^{\Upsilon}(0,t) = 0, \quad \sigma_{\Upsilon}(L,t) = \frac{A}{L}\left(-\sum_{j=1}^{N_p} \frac{\gamma_j}{\tau_j} e^{-(t-\Upsilon)/\tau_j}\right), \\ &s^{\Upsilon}(x,0) = 0, \quad (s^{\Upsilon})_t(x,0) = 0, \end{aligned} \tag{A.7a}$$

In the above equation, the sensitivity of stress with respect to Υ (i.e., σ_{Υ}) is given by

$$\sigma_{\Upsilon} \quad = \quad E_1(s^{\Upsilon})_{xt} + \left(E + \sum_{j=1}^{N_p}\gamma_j\right)(s^{\Upsilon})_x - \sum_{j=1}^{N_p}\gamma_j\epsilon^j_{\Upsilon}. \tag{A.7b}$$

The sensitivity of the internal variabl ϵ^j with respect to Υ (i.e., $\epsilon^j_{\Upsilon} = \dfrac{\partial \epsilon^j}{\partial \Upsilon}$) satisfies, for $j = 1, \ldots, N_p$,

$$\tau_j(\epsilon^j_{\Upsilon})_t + \epsilon^j_{\Upsilon} = (s^{\Upsilon})_x, \quad \epsilon^j_{\Upsilon}(0) = 0. \tag{A.7c}$$

A.2 Shear Model

1. Sensitivity PDE for ρ (where $s^{\rho} = \dfrac{\partial u}{\partial \rho}$):

$$\begin{aligned} &\rho(s^{\rho})_{tt} - (\sigma_{\rho})_r - \frac{\sigma_{\rho}}{r} = -u_{tt} \\ &\sigma_{\rho}(r_{min},t) = 0, \quad s^{\rho}(r_{max},t) = 0, \\ &s^{\rho}(r,0) = 0, \quad (s^{\rho})_t(r,0) = 0, \end{aligned} \tag{A.8a}$$

In the above equation, the sensitivity of stress with respect to ρ (i.e., σ_{ρ}) is given by

$$\sigma_{\rho} \quad = \quad G_1(s^{\rho})_{rt} + \left(G + \sum_{j=1}^{N_p}\zeta_j\right)(s^{\rho})_r - \sum_{j=1}^{N_p}\zeta_j\epsilon^j_{\rho}. \tag{A.8b}$$

The sensitivity of the internal variabl ϵ^j with respect to ρ (i.e., $\epsilon^j_{\rho} = \dfrac{\partial \epsilon^j}{\partial \rho}$) satisfies (for $j = 1, \ldots, N_p$).

$$\tau_j(\epsilon^j_{\rho})_t + \epsilon^j_{\rho} = (s^{\rho})_r, \quad \epsilon^j_{\rho}(0) = 0. \tag{A.8c}$$

2. Sensitivity PDE for G (where $s^{G} = \dfrac{\partial u}{\partial G}$):

$$\begin{aligned} &\rho(s^{G})_{tt} - (\sigma_{G})_r - \frac{\sigma_{G}}{r} = 0 \\ &\sigma_{G}(r_{min},t) = 0, \quad s^{G}(r_{max},t) = 0, \\ &s^{G}(r,0) = 0, \quad (s^{G})_t(r,0) = 0, \end{aligned} \tag{A.9a}$$

In the above equation, the sensitivity of stress with respect to G (i.e., σ_{G}) is given by

$$\sigma_{G} \quad = \quad G_1(s^{G})_{rt} + \left(G + \sum_{j=1}^{N_p}\zeta_j\right)(s^{G})_r - \sum_{j=1}^{N_p}\zeta_j\epsilon^j_{G} + u_r. \tag{A.9b}$$

The sensitivity of the internal variabl ϵ^j with respect to G (i.e., $\epsilon^j_{G} = \dfrac{\partial \epsilon^j}{\partial G}$) satisfies, for $j = 1, \ldots, N_p$,

$$\tau_j(\epsilon^j_{G})_t + \epsilon^j_{G} = (s^{G})_r, \quad \epsilon^j_{G}(0) = 0. \tag{A.9c}$$

3. Sensitivity PDE for G_1 (where $s^{G_1} = \dfrac{\partial u}{\partial G_1}$):

$$\begin{aligned}
&\rho(s^{G_1})_{tt} - (\sigma_{G_1})_r - \frac{\sigma_{G_1}}{r} = 0 \\
&\sigma_{G_1}(r_{min}, t) = 0, \quad s^{G_1}(r_{max}, t) = 0, \\
&s^{G_1}(r, 0) = 0, \quad (s^{G_1})_t(r, 0) = 0,
\end{aligned} \tag{A.10a}$$

In the above equation, the sensitivity of stress with respect to G_1 (i.e., σ_{G_1}) is given by

$$\sigma_{G_1} \;=\; G_1(s^{G_1})_{rt} + \left(G + \sum_{j=1}^{N_p} \zeta_j\right)(s^{G_1})_r - \sum_{j=1}^{N_p} \zeta_j \epsilon^j_{G_1} + u_{rt}. \tag{A.10b}$$

The sensitivity of the internal variabl ϵ^j with respect to G_1 (i.e., $\epsilon^j_{G_1} = \dfrac{\partial \epsilon^j}{\partial G_1}$) satisfies, for $j = 1, \ldots, N_p$,

$$\tau_j(\epsilon^j_{G_1})_t + \epsilon^j_{G_1} = (s^{G_1})_r, \quad \epsilon^j_{G_1}(0) = 0. \tag{A.10c}$$

4. Sensitivity PDE for τ_k (where $s^{\tau_k} = \dfrac{\partial u}{\partial \tau_k}$):

$$\begin{aligned}
&\rho(s^{\tau_k})_{tt} - (\sigma_{\tau_k})_r - \frac{\sigma_{\tau_k}}{r} = \frac{1}{r}\frac{A}{r_{max} - r_{min}}\left(t\frac{\zeta_k}{\tau_k^2}e^{-t/\tau_k} - (t-\Upsilon)\frac{\zeta_k}{\tau_k^2}e^{-(t-\Upsilon)/\tau_k}\right) \\
&\sigma_{\tau_k}(r_{min}, t) = -\frac{A}{r_{max} - r_{min}}\left(t\frac{\zeta_k}{\tau_k^2}e^{-t/\tau_k} - (t-\Upsilon)\frac{\zeta_k}{\tau_k^2}e^{-(t-\Upsilon)/\tau_k}\right), \quad s^{\tau_k}(r_{max}, t) = 0, \\
&s^{\tau_k}(r, 0) = 0, \quad (s^{\tau_k})_t(r, 0) = 0,
\end{aligned} \tag{A.11a}$$

In the above equation, the sensitivity of stress with respect to τ_k (i.e., σ_{τ_k}) is given by

$$\sigma_{\tau_k} \;=\; G_1(s^{\tau_k})_{rt} + \left(G + \sum_{j=1}^{N_p} \zeta_j\right)(s^{\tau_k})_r - \sum_{j=1}^{N_p} \zeta_j \epsilon^j_{\tau_k}. \tag{A.11b}$$

The sensitivity of the internal variabl ϵ^j with respect to τ_k (i.e., $\epsilon^j_{\tau_k} = \dfrac{\partial \epsilon^j}{\partial \tau_k}$) satisfies, for $j = 1, \ldots, N_p$,

- if $j = k$ then

$$\tau_k(\epsilon^k_{\tau_k})_t + \epsilon^k_{\tau_k} = (s^{\tau_k})_r - \epsilon^k_t, \quad \epsilon^k_{\tau_k}(0) = 0, \tag{A.11c}$$

- if $j \neq k$ then

$$\tau_j(\epsilon^j_{\tau_k})_t + \epsilon^j_{\tau_k} = (s^{\tau_k})_r, \quad \epsilon^j_{\tau_k}(0) = 0. \tag{A.11d}$$

5. Sensitivity PDE for ζ_k (where $s^{\zeta_k} = \dfrac{\partial u}{\partial \zeta_k}$):

$$\begin{aligned}
&\rho(s^{\zeta_k})_{tt} - (\sigma_{\zeta_k})_r - \frac{\sigma_{\zeta_k}}{r} = \frac{1}{r}\frac{A}{r_{max} - r_{min}}\left(e^{-t/\tau_k} - e^{-(t-\Upsilon)/\tau_k}\right) \\
&\sigma_{\zeta_k}(r_{min}, t) = -\frac{A}{r_{max} - r_{min}}\left(e^{-t/\tau_k} - e^{-(t-\Upsilon)/\tau_k}\right), \quad s^{\zeta_k}(r_{max}, t) = 0 \\
&s^{\zeta_k}(r, 0) = 0, \quad (s^{\zeta_k})_t(r, 0) = 0,
\end{aligned} \tag{A.12a}$$

In the above equation, the sensitivity of stress with respect to ζ_k (i.e., σ_{ζ_k}) is given by

$$\sigma_{\zeta_k} \;=\; G_1(s^{\zeta_k})_{rt} + \left(G + \sum_{j=1}^{N_p} \zeta_j\right)(s^{\zeta_k})_r - \sum_{j=1}^{N_p} \zeta_j \epsilon^j_{\zeta_k} + u_r - \epsilon^k. \tag{A.12b}$$

The sensitivity of the internal variabl ϵ^j with respect to ζ_k (i.e., $\epsilon^j_{\zeta_k} = \dfrac{\partial \epsilon^j}{\partial \zeta_k}$) satisfies, for $j = 1, \ldots, N_p$,

$$\tau_j(\epsilon^j_{\zeta_k})_t + \epsilon^j_{\zeta_k} = (s^{\zeta_k})_r, \quad \epsilon^j_{\zeta_k}(0) = 0. \tag{A.12c}$$

6. Sensitivity PDE for A (where $s^A = \dfrac{\partial u}{\partial A}$):

$$
\begin{aligned}
&\rho(s^A)_{tt} - (\sigma_A)_r - \frac{\sigma_A}{r} = \frac{1}{r}\frac{1}{r_{max}-r_{min}}\left(\sum_{j=1}^{N_p}\zeta_j e^{-t/\tau_j} - \sum_{j=1}^{N_p}\zeta_j e^{-(t-\Upsilon)/\tau_j}\right)\\
&\sigma_A(r_{min},t) = -\frac{1}{r_{max}-r_{min}}\left(\sum_{j=1}^{N_p}\zeta_j e^{-t/\tau_j} - \sum_{j=1}^{N_p}\zeta_j e^{-(t-\Upsilon)/\tau_j}\right), \quad s^A(r_{max},t) = 0\\
&s^A(r,0) = \frac{r_{max}-r}{r_{max}-r_{min}}, \quad (s^A)_t(r,0) = 0,
\end{aligned}
\tag{A.13a}
$$

In the above equation, the sensitivity of stress with respect to A (i.e., σ_A) is given by

$$
\sigma_A \quad = \quad G_1(s^A)_{rt} + \left(G + \sum_{j=1}^{N_p}\zeta_j\right)(s^A)_r - \sum_{j=1}^{N_p}\zeta_j \epsilon_A^j. \tag{A.13b}
$$

The sensitivity of the internal variables ϵ^j with respect to A (i.e., $\epsilon_A^j = \dfrac{\partial \epsilon^j}{\partial A}$) satisfies, for $j = 1, \ldots, N_p$,

$$
\tau_j(\epsilon_A^j)_t + \epsilon_A^j = (s^A)_r, \quad \epsilon_A^j(0) = 0. \tag{A.13c}
$$

7. Sensitivity PDE for Υ (where $s^\Upsilon = \dfrac{\partial u}{\partial \Upsilon}$):

$$
\begin{aligned}
&\rho(s^\Upsilon)_{tt} - (\sigma_\Upsilon)_r - \frac{\sigma_\Upsilon}{r} = \frac{1}{r}\frac{A}{r_{max}-r_{min}}\left(-\sum_{j=1}^{N_p}\frac{\zeta_j}{\tau_j} e^{-(t-\Upsilon)/\tau_j}\right)\\
&\sigma_\Upsilon(r_{min},t) = -\frac{A}{r_{max}-r_{min}}\left(-\sum_{j=1}^{N_p}\frac{\zeta_j}{\tau_j} e^{-(t-\Upsilon)/\tau_j}\right), \quad s^\Upsilon(r_{max},t) = 0\\
&s^\Upsilon(r,0) = 0, \quad (s^\Upsilon)_t(r,0) = 0,
\end{aligned}
\tag{A.14a}
$$

In the above equation, the sensitivity of stress with respect to Υ (i.e., σ_Υ) is given by

$$
\sigma_\Upsilon \quad = \quad G_1(s^\Upsilon)_{rt} + \left(G + \sum_{j=1}^{N_p}\zeta_j\right)(s^\Upsilon)_r - \sum_{j=1}^{N_p}\zeta_j \epsilon_\Upsilon^j. \tag{A.14b}
$$

The sensitivity of the internal variables ϵ^j with respect to Υ (i.e., $\epsilon_\Upsilon^j = \dfrac{\partial \epsilon^j}{\partial \Upsilon}$) satisfies, for $j = 1, \ldots, N_p$,

$$
\tau_j(\epsilon_\Upsilon^j)_t + \epsilon_\Upsilon^j = (s^\Upsilon)_r, \quad \epsilon_\Upsilon^j(0) = 0. \tag{A.14c}
$$